J. Physiol. (1981), **312**, *pp.* 377–412
With 16 text-figures
Printed in Great Britain

AN ELECTRICAL TUNING MECHANISM IN TURTLE COCHLEAR HAIR CELLS

BY A. C. CRAWFORD AND R. FETTIPLACE

From the Physiological Laboratory, University of Cambridge, Downing Street, Cambridge

(*Received 30 April 1980*)

SUMMARY

1. Intracellular recordings were made from single cochlear hair cells in the isolated half-head of the turtle. The electrical responses of the cells were recorded under two conditions: (a) when the ear was stimulated with low-intensity tones of different frequencies and (b) when current steps were injected through the intracellular electrode. The aim of the experiments was to evaluate the extent to which the cochlea's frequency selectivity could be accounted for by the electrical properties of the hair cells.

2. At low levels of acoustic stimulation, the amplitude of the hair cell's receptor potential was proportional to sound pressure. The linear tuning curve, which is defined as the sensitivity of the cell as a function of frequency when the cell is operating in its linear range, was measured for a number of hair cells with characteristic frequencies from 86 Hz to 425 Hz.

3. A rectangular current passed into a hair cell elicited a membrane potential change consisting of a damped oscillation superimposed on a step. Small currents produced symmetrical oscillations at the beginning and end of the pulse. Larger currents increased the initial ringing frequency if depolarizing and decreased it if hyperpolarizing.

4. For small currents the frequency of the oscillations and the quality factor (Q) of the electrical resonance derived from the decay of the oscillations were close to the characteristic frequency and Q of the hair-cell linear tuning curve obtained from sound presentations.

5. The hair cell's membrane potential change to small-current pulses or low-intensity tone bursts could be largely described by representing the hair cell as a simple electrical resonator consisting of an inductance, resistor and capacitor.

6. When step displacements of 29–250 nm were applied to a micropipette, placed just outside a hair cell in the basilar papilla, an initial periodic firing of impulses could be recorded from single fibres in the auditory nerve. Currents of up to 1 nA, injected through the same micropipette, failed to produce any change in the auditory nerve discharge. The experiment demonstrates that current injection does not produce gross movements of the electrode tip.

7. The contribution of the electrical resonance to hair-cell tuning was assessed by dividing the linear tuning curve by the cell's impedance as a function of frequency.

0022-3751/81/3760-0953 $07.50

The procedure assumes that the electrical resonance is independent of other filtering stages, and on this assumption the resonance can account for the tip of the acoustical tuning curve.

8. The residual filter produced by the division was broad; it exhibited a high-frequency roll-off with a corner frequency at 500–600 Hz, similar in all cells, and a low-frequency roll-off, with a corner frequency from 30 to 350 Hz which varied from cell to cell but was uncorrelated with the characteristic frequency of the cell.

9. The phase of the receptor potential relative to the sound pressure at the tympanum was measured in ten cells. For low intensities the phase characteristic was independent of the sound pressure. At low frequencies the receptor potential led the sound by 270–360°, and in the region of the characteristic frequency there was an abrupt phase lag of 90–180°; the abruptness of the phase change depended upon the Q of the cell.

10. The calculated phase shift of the electrical resonator as a function of frequency was subtracted from the phase characteristic of the receptor potential. The subtraction removed the sharp phase transition around the characteristic frequency, and in this frequency region the residual phase after subtraction was approximately constant at +180°. This is consistent with the idea that the hair cells depolarize in response to displacements of the basilar membrane towards the scala vestibuli. The high-frequency region of the residual phase characteristic was similar in all cells.

11. It is concluded that each hair cell contains its own electrical resonance mechanism which accounts for most of the frequency selectivity of the receptor potential. All cells also show evidence of a broad band-pass filter, the high frequency portion of which may be produced by the action of the middle ear.

INTRODUCTION

The basilar membrane in reptiles is extremely small in comparison with that of mammals, and for orders other than *Crocodilia* achieves a maximum length of less than about 2·0 mm (Wever, 1978; Miller, 1978*a*, *b*; Manley, 1971). In spite of this, the reptilian cochlea is capable of a high degree of frequency selectivity, which is reflected in the sharp tuning of responses from single auditory nerve fibres (Weiss, Mulroy, Turner & Pike, 1976; Manley, 1977; Crawford & Fettiplace, 1980*a*) and hair cells (Crawford & Fettiplace, 1980*a*). The sensory cells are tonotopically organized along the cochlea according to the frequency to which they are most sensitive (Weiss, Peake, Ling & Holton, 1978; Crawford & Fettiplace, 1980*a*) but the rate of change of frequency with position seems too great for the tuning to be explained solely by variations in the mechanical properties of the membrane (Crawford & Fettiplace, 1980*a*); for one reptile, measurements of the vibration of the basilar membrane have revealed that its motion contributes little to the frequency selectivity (Weiss *et al.* 1978). This suggests that a frequency-selective mechanism may operate subsequent to the basilar membrane vibration, perhaps in the hair cells themselves. The origin of the frequency selectivity is of more than comparative interest, for even in the mammalian cochlea it has been proposed that a tuning mechanism other than that endowed by the mechanical response of the basilar membrane must be present in order to generate the sharp selectivity of the auditory nerve fibres (Evans, 1972; Evans & Wilson, 1973; Geisler, Rhode & Kennedy, 1974).

Recently, we have developed an *in vitro* preparation of the turtle's cochlea, which has enabled us to record intracellularly the responses of single hair cells (Fettiplace & Crawford, 1978; Crawford & Fettiplace, 1980*a*). We found that the form and tuning of the responses display a number of properties akin to a simple resonance exemplified by an electrical filter containing an inductance, resistance and capacitance. In addition, a resonance phenomenon can be observed on injecting current into a single cell, which has led us to suggest that each hair cell contains its own tuning mechanism (Fettiplace & Crawford, 1978).

In this paper we will describe in detail the behaviour of the electrical resonance revealed by current injection and evaluate the extent to which it can account for the tuning and phase of the hair cell's receptor potential to low-intensity sound stimuli. In a later paper (Crawford & Fettiplace, 1980*b*) we will examine the non-linearities that can shape the receptor potential at high sound intensities.

Some of the results described in this paper have been published previously in a preliminary form (Crawford & Fettiplace, 1978; Fettiplace & Crawford, 1978, 1980).

METHODS

Preparation and recording techniques. Most of the techniques have been described in detail elsewhere (Crawford & Fettiplace, 1980*a*). Experiments were performed on the isolated cochlea of the turtle *Pseudemys scripta elegans* (carapace length 30–35 mm). After decapitation the head was split in the mid line, the brain removed and the scala tympani opened from the cranial side. The tympanum was sealed to an acoustic coupler connected to an earphone and monitoring microphone, and the whole preparation was mounted in a chamber gassed with a moist 95 %/5 % O_2/CO_2 mixture.

Micropipettes filled with 4 M-potassium acetate (resistances 300–500 MΩ) were advanced into the bases of hair cells from the scala tympani and potentials measured with respect to an earthed silver–silver chloride half-cell connected via a Ringer bridge to the auditory nerve.

Currents up to 1·0 nA, injected into hair cells down the recording electrode using a constant current source based on the circuit of Fein (1966) and Colburn & Schwartz (1972), were monitored by measuring the potential drop across a 100 MΩ resistor in series with the micro-electrode. The rise time of the current was faster than 10 μsec for the current range used. To measure the hair cell potential during current injection, the potential drop across the electrode resistance was balanced out with a bridge circuit; the balance point was assessed in each experiment with the electrode inside a cell from the knee on the rising phase of the potential step to a small current pulse. In every experiment the band width of the recording system was determined by passing a sinusoidal current (100 pA peak-to-peak) down the recording electrode, placed just outside the hair cell, and measuring the potential drop across the electrode resistance as a function of frequency, from 5 Hz to 5 kHz. The deficiencies of this method are discussed in Crawford & Fettiplace (1980*a*), where examples of the calibration procedure are also given. The capacity compensation applied to the input of the electrometer achieved a 3 dB band width for the recording system of about 3 kHz under the best circumstances, but often the band width was only a third of this. Intracellular potentials from hair cells were recorded using an FM tape recorder (tape speed 15 in/sec, band width 5 kHz) for subsequent analysis.

The sound delivery system. This was similar to that described by Crawford & Fettiplace (1980*a*). Tonal stimuli consisting either of swept-frequency tones (10 Hz–3 kHz) or of tone bursts possessing an integral number of half-cycles were generated by a Beyer DT 505 or DT 48 earphone. With a constant driving signal delivered to the earphone the sound pressure at the tympanum was constant (±10 dB) over the frequency range used. For swept-tones second harmonic distortion in the sound stimulus was more than 60 dB below the fundamental for sound pressures below 120 dB s.p.l.; for tone bursts the second harmonic was more than 50 dB below the fundamental over the same intensity range. The sound pressure at the tympanum was monitored continuously throughout an experiment using a ½ in. Bruel & Kjaer condenser microphone, calibrated probe tube, and Bruel & Kjaer 2608 measuring amplifier. In a few experiments tone bursts were tapered by passing the electrical driving signal through six-pole Butterworth high- and low-pass active filters with a

common cut-off frequency, which served to reduce the harmonic distortion in the electrical signal to levels well below those generated by the earphone. All stimulus intensities are expressed as a sound pressure level in decibels with respect to 20 μPa (dB s.p.l.).

Phase measurements. The phase of the hair cell potential was measured relative to that of the pressure wave at the tympanum using a pair of Brookdeal 9503-SC phase-lock amplifiers and 5042 Omniphase unit; the phase-lock amplifiers were referenced in quadrature to the electrical signal delivered to the earphone. The outputs of the phase-lock amplifiers were the r.m.s. values of the

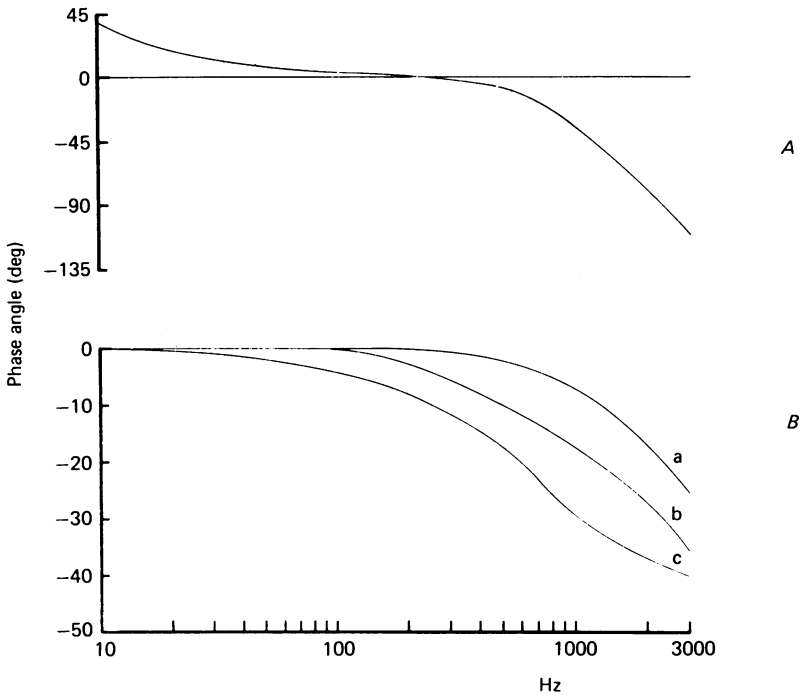

Fig. 1. Phase corrections. *A*, phase shift introduced by the sound monitoring system (with respect to the sound pressure at the tympanum) with the convention that a positive angle represents a lead; the phase lead at low frequency is due to the condenser microphone, preamplifier and measuring amplifier. The lag at frequencies above 300 Hz is contributed by the probe tube. *B*, phase shifts introduced by the recording system in three different experiments. These were obtained with the intracellular electrode just outside a hair cell by injecting a 0·1 nA sinusoidal current whose frequency was swept from 10 Hz to 3 kHz. The low-frequency resistance of the intracellular electrode was: a, 208 MΩ; b, 340 MΩ; c, 585 MΩ. The frequency scale on the abscissa applies to both *A* and *B*.

components of the hair-cell response which were in phase and 90° out of phase relative to the reference signal, and from these, the Omniphase unit generated voltages proportional to the modulus and phase of the hair cell response. All phase measurements are based on the convention that a compression and a depolarization of the hair cell are considered to be positive quantities. The total phase angle at any frequency, $\Theta_{vs}(\omega)$, is given by

$$\Theta_{vs}(\omega) = \Theta_{v}(\omega) - \Theta_{s}(\omega), \quad (1)$$

where $\Theta_{v}(\omega)$ is the phase of the hair cell receptor potential and $\Theta_{s}(\omega)$ is the phase of the pressure wave at the tympanum, both measured relative to the electrical driving signal delivered to the earphone. Unless otherwise stated $\Theta_{vs}(\omega)$ is a lead if positive and a lag if negative.

A number of subsequent corrections for the instrumental phase contributions had to be applied to $\Theta_{vs}(\omega)$ to obtain the true phase angle of the biological system.

1. The preamplifier and measuring amplifier introduced a phase lead in the sound signal at low frequencies which was measured by connecting a 20 pF capacitor (using a Bruel & Kjaer JJ2615 adaptor) to the preamplifier to simulate the microphone cartridge and delivering constant voltage signals to the input.

2. The condenser microphone cartridge also introduced a low-frequency phase lead due to the pressure equalization mechanism. The correction, $\Theta'(f)$, can be calculated from $\Theta'(f) = \tan^{-1}(f/f_0)$ where f is the frequency and f_0 is the lower corner frequency of the pressure response of the microphone, given by the makers as about 2 Hz.

3. To correct for the phase lag in the sound monitor introduced by the probe tube a second condenser microphone was sealed into the experimental chamber in the position normally occupied by the tympanum. The phase difference between the probe microphone signal and the reference microphone signal was used to obtain the true phase of the pressure wave for frequencies above 200 Hz.

The combined correction for the effects described in 1–3 above is given in Fig. 1*A*.

4. The recording system introduced a variable phase lag as the frequency increased, dependent both on the electrode resistance and the degree of capacity neutralization applied to the electrometer. For each recording a phase calibration procedure was performed similar to the calibration given for the gain of the recording system; the phase of the voltage drop across the electrode resistance was measured with respect to the phase of a sinusoidal swept-frequency current (100 pA peak-to-peak) injected down the electrode, which was placed just outside the hair cell at the end of a recording. The capacity compensation, adjusted at the beginning of the recording with the electrode positioned inside the cell, was not altered again until the phase calibration procedure had been executed. Fig. 1*B* gives examples of the phase shift of the recording system for three different experiments. Since the electrode resistance may increase slightly on penetrating a cell, it is likely that our calibration procedure underestimates the phase lag introduced by the electrode. Phase corrections given in Fig. 1*A* for the sound system are added to the value of $\Theta_{vs}(\omega)$, and phase corrections for the recording system are subtracted from the value of $\Theta_{vs}(\omega)$, so to some extent the corrections cancel in the frequency decade from 100 Hz to 1 kHz.

Measurements of acoustic tuning. The procedure used was similar to that given in Crawford & Fettiplace, 1980*a*. Swept-frequency tones were presented at various constant intensities and the modulus of the receptor potential was measured using two phase-lock amplifiers referenced in quadrature. Sound pressures producing a response at the characteristic frequency of the cell of less than about 2 mV in amplitude, generated iso-intensity response curves in the hair cell that had a constant form and were superimposable by scaling by the sound pressure. The resulting common curve, which we call the linear tuning curve, relates the sensitivity of the cell (in mV/Pa, both as r.m.s. values) to frequency, and represents our best estimate of the frequency selectivity of the hair cell operating in its linear range. Examples of linear tuning curves are given in Fig. 11.

Imposed mechanical displacements of the recording electrode. The micro-electrode was mechanically displaced by mounting it on the diaphragm of a Danavox wide-band miniature earphone, which produced a displacement of the electrode mainly along its main axis, although some lateral movement of the tip inevitably occurred because the electrodes used in these experiments always possessed some curvature. The movement of the electrode was calibrated under stroboscopic illumination with the tip dipping 300–400 μm into water (approximately the depth of the fluid in the scala tympani). Displacement was found to be a linear function of the voltage delivered to the earphone in the range 5–50 μm and is assumed to remain linear for smaller driving signals.

The frequency response of the displacement of the electrode was dominated by its lateral resonances and not by resonances of the earphone. For the electrodes used, the principal resonant frequencies lay in the range 1–5 kHz (electrode shank length, 15–25 mm) with the higher modes of vibration dominating. The resonant frequencies were not harmonically related since the stiffness and mass per unit length vary with distance along the shank. Below 1 kHz, the displacement amplitude of the electrode was largely independent of the frequency of vibration.

THEORY

A number of features of the hair cell's voltage responses can be described by assuming that the cell behaves like an electrical resonator. The aim of this section

is to collect together the equations needed for this description. Subsequent sections will show that these equations can largely describe the response of the cell to injection of currents down the micro-electrode, and the amplitude and phase of the cell's response to sound stimulation. The analysis presented is a linear one, and is only applicable to small responses less than a few millivolts in amplitude which are in the linear range. It does not account for the non-linearities that occur with large voltage excursions.

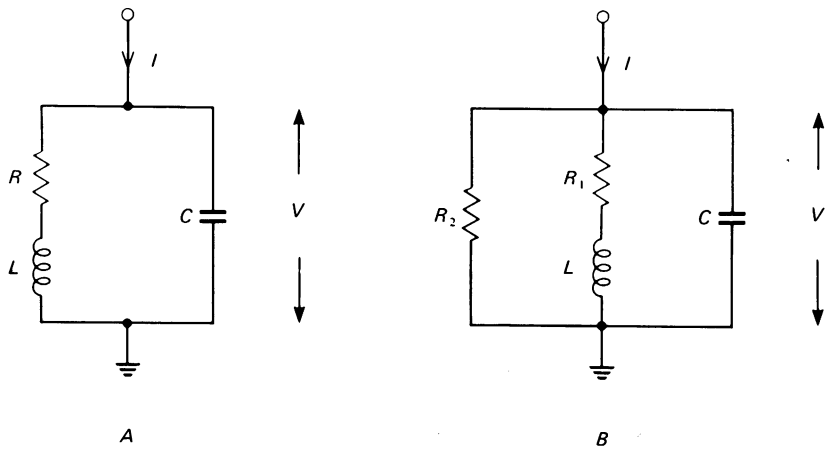

Fig. 2. *A*, equivalent circuit used to describe the electrical resonance in a hair cell. The input is a current, I, from a high-impedance source, and the output is the voltage, V, across the capacitor. *B*, equivalent circuit representing the small-signal behaviour of a voltage-sensitive conductance for voltages positive to the equilibrium potential of the conducting ion, and where the conductance is turned on by depolarization.

The type of resonance which best fits the results has an equivalent circuit shown in Fig. 2*A*. The circuit is composed of a capacitor, C, in parallel with a series combination of an inductance, L, and resistor R. The input is a current, I (from a high-impedance source) and the output is the voltage, V, across the capacitor. The differential equation for the circuit is given by:

$$\ddot{V}+\gamma\dot{V}+\omega_0^2 V=\frac{\gamma I}{C}+\frac{\dot{I}}{C}, \tag{2}$$

where the dot indicates differentiation with respect to time; γ and ω_0 are the damping constant and resonant angular frequency of the filter respectively and are related to the circuit parameters by:

$$\gamma = R/L$$
$$\omega_0^2 = 1/LC. \tag{3}$$

The sharpness of tuning of the filter can be expressed in terms of the quality factor, Q, which is a dimensionless constant given by:

$$Q=\frac{\omega_0}{\gamma}. \tag{4}$$

Two other configurations of the *LRC* circuit were considered but had properties

that were inconsistent with the hair cell membrane potential changes to rectangular current pulses. (1) If the inductance, resistor and capacitor are all connected in parallel, then the voltage across the circuit is zero at very low frequencies and at very high frequencies and there is no steady response to a current step. (2) If the inductance, resistor and capacitor are connected in series and driven by a constant voltage source, then the output voltage across the capacitor is correct qualitatively, but the phases of the voltage oscillations relative to the start of a step input are incorrect; the peaks in the step response of the series circuit occur at π, 3π, $5\pi \ldots (2n+1)\pi$ radians, whereas the circuit of Fig. 2 *A*, in the limit of a high quality factor, has a step response consisting of damped oscillations with peaks at $\pi/2$, $5\pi/2$, $9\pi/2 \ldots (2n+\frac{1}{2})\pi$ radians. The latter behaviour most closely describes the experimental results (see Fig. 7).

Responses to a sinusoidal input

If the input to the filter is a sinusoidal current, generated by the mechano-electrical transduction mechanism in response to a low-intensity tone burst, I has the form:

$$\begin{aligned} I &= \bar{I} \sin \omega t \quad t \geqslant 0 \\ &= 0 \qquad\quad t < 0 \end{aligned} \tag{5}$$

and the solution to eqn. (2) for the boundary conditions imposed by eqn. (5) (namely $V = \dot{V} = 0$ at $t = 0$) is

$$\begin{aligned} V = {} & \frac{\bar{I}}{\lambda^2 C}\{\omega_0^2 \gamma \sin \omega t - [\omega(\gamma^2 + \omega^2 - \omega_0^2)] \cos \omega t\} \\ & - \frac{\bar{I}}{\lambda^2 C} e^{-\gamma t/2} \left\{ \frac{\omega\gamma}{2\omega_f} [3\omega_0^2 - \gamma^2 - \omega^2] \sin \omega_f t - [\omega(\gamma^2 + \omega^2 - \omega_0^2)] \cos \omega_f t \right\} \end{aligned} \tag{6}$$

with

$$\lambda^2 = (\omega_0^2 - \omega^2)^2 + \gamma^2 \omega^2$$

where w_f is given by

$$\omega_f = \omega_0 \left(1 - \frac{1}{(2Q)^2}\right)^{\frac{1}{2}}, \quad (\gamma < 2\omega_0) \tag{7}$$

For $\omega = \omega_f$ and Q large, eqn. (6) reduces to

$$V = \frac{\bar{I}}{\gamma C} \sin(\omega_f t - \alpha)\{1 - e^{-\gamma t/2}\}, \quad \alpha = \tan^{-1} \frac{3}{4Q}. \tag{8}$$

Eqn. (8) is similar to eqn. (15) of Crawford & Fettiplace (1980*a*) which was used to describe the exponential build-up of the response of a hair cell to a low-intensity tone burst at the cell's characteristic frequency.

Eqn. (6) consists of two main terms, the first describing the steady-state behaviour and the second containing the transient contribution. If the duration of the stimulus is long compared to $2/\gamma$, the output voltage may be put in the form

$$V = A(\omega) \sin(\omega t + \phi(\omega)), \tag{9}$$

where A and ϕ are the amplitude and phase characteristics of the resonant filter, and are given by

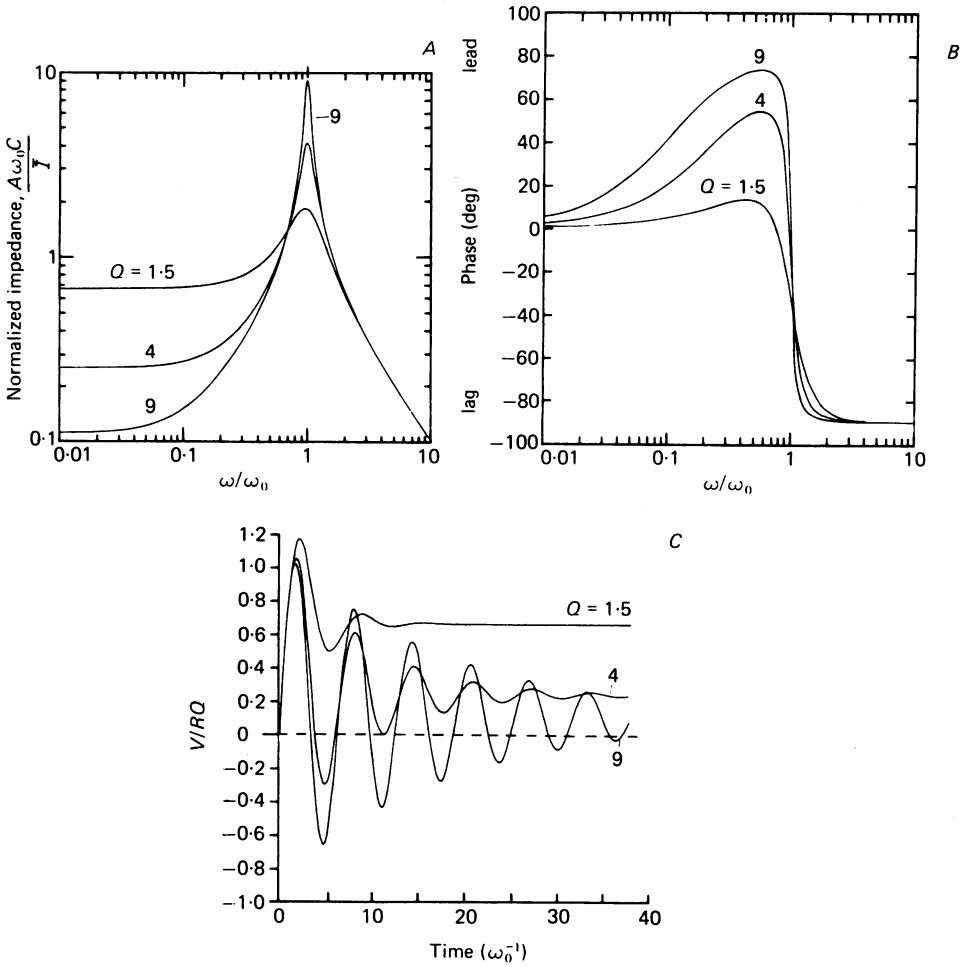

Fig. 3. Theoretical behaviour of the electrical circuit in Fig. 2*A* for a sinusoidal current input (*A* and *B*) and a step input (*C*). In Fig. 3*A*, the normalized impedance, $A\omega_0 C/\bar{I}$, of the filter is plotted against the angular frequency, ω, of the sinusoidal current scaled to the circuits resonant angular frequency, ω_0. The curves have been calculated from eqn. (10) for three different values of the quality factor, Q, the value of Q being given beside each trace. In Fig. 3*B* the phase of the output voltage across the capacitor relative to the current input is plotted against the normalized angular frequency of the current; the curves have been calculated from eqn. (11) for the same values of Q. In *C*, the voltage onset, calculated from eqn. (13), for a unit current step input is plotted with the three values of Q. The ordinate in *C* is V/RQ, where V is the voltage across the capacitor and R is the value of the resistor in the circuit in Fig. 2*A*.

$$A(\omega) = \frac{\bar{I}}{\omega_0 C}\left\{\frac{Q^2+\omega_0^2/\omega^2}{\left(\frac{\omega}{\omega_0}-\frac{\omega_0}{\omega}\right)^2 Q^2+1}\right\}^{\frac{1}{2}} \tag{10}$$

$$\phi(\omega) = \tan^{-1}\left\{\frac{\omega Q}{\omega_0}-\frac{\omega^3 Q}{\omega_0^3}-\frac{\omega}{\omega_0 Q}\right\}. \tag{11}$$

The amplitude and phase behaviour as a function of ω/ω_0 are illustrated in Fig. 3*A* and *B*. The curves have been calculated using eqns. (10) and (11) for three different

values of the quality factor, Q, equal to 1·5, 4 and 9. For the amplitude curve, the ordinate is the normalized impedance $A\omega_0 C/\bar{I}$. The normalized impedance is the impedance of the resonant circuit multiplied by the admittance, $\omega_0 C$, and is a dimensionless variable which will be used later in the paper to assess the contribution of the electrical resonance to hair-cell tuning. This normalization was adopted because it allows the relative gain of the filter to be specified solely in terms of ω_0 and Q.

Several features are worth noting about the curves in Fig. 3*A*, *B*. From the amplitude plots, it can be seen that the normalized impedance at low frequency is constant and given by $1/Q$, whereas at ω_0 it is $(1+Q^2)^{\frac{1}{2}}$. At high frequencies all curves converge, the gain declining with a limiting slope of -1. The phase curves are striking in that they exhibit an increasing phase lead which reaches a maximum, for large Q, at about $\omega_0/\sqrt{3} = 0{\cdot}577\,\omega_0$. Around ω_0 there is a rapid increment in phase lag of between 90 and 180°, and at high frequencies all curves asymptotically approach a lag of 90°.

Responses to current steps

The features of the resonant circuit can also be revealed by injecting rectangular current steps. The input, I, then has the form

$$I = \bar{I}u(t), \tag{12}$$

where $\bar{I}$ is the magnitude of the current step and $u(t)$ is the unit step function ($u(t) = 0$, $t < 0$; $u(t) = 1$, $t \geqslant 0$). The solution to eqn. (2) for this kind of input is:

$$V_u = \bar{I}R\left\{1 + \frac{\omega_0^2}{\omega_f\gamma}\, e^{-\gamma t/2} \sin(\omega_f t - \phi')\right\} \tag{13}$$

$$\phi' = \sin^{-1}\frac{\omega_f\gamma}{\omega_0^2}.$$

For large Q, $\omega_0 \simeq \omega_f$, and eqn. (13) simplifies to

$$V_u = \bar{I}R\{1 + Qe^{-\gamma t/2} \sin(\omega_f t - \phi')\} \tag{14}$$

$$\phi' = \tan^{-1}\frac{1}{Q}.$$

The form of the response given by eqn. (13) is shown in Fig. 3*C* for the three values of Q which were used for the amplitude and phase curves. The response consists of a voltage step, upon which is superimposed damped oscillations at the frequency $\omega_f/2\pi$. From measurements of the frequency of the oscillations and the time constant of their decay ($2/\gamma$) it is thus possible to reconstruct the filter. The information gleaned from the step response is directly equivalent to that obtained from amplitude and phase measurements as a function of frequency, and contains everything needed to specify the filter.

The voltage response of the hair cell to extrinsic current steps of duration T will be fitted by:

$$V = V_u(t) - V_u(t-T), \tag{15}$$

where V_u is given by eqn. (13). If the duration, T, of the input becomes very short, V is approximated by the impulse response of the resonant filter given by:

$$V = \frac{I\Delta t}{C}\left\{1+\frac{\gamma^2}{4\omega_f^2}\right\}^{\frac{1}{2}} e^{-\gamma t/2}\cos(\omega_f t-\phi'') \tag{16}$$

$$\phi'' = \tan^{-1}\frac{\gamma}{2\omega_f}$$

$$\simeq \tan^{-1}\frac{1}{2Q} \quad \text{for large } Q.$$

$I\Delta t$ is the charge deposited on the capacitor at $t = 0$. The equation has the same form as eqn. (17) of Crawford & Fettiplace (1980*a*) which was used to fit the hair cell's responses to clicks.

Parallel resonance with two resistances

The physical basis of the electrical resonance circuit of Fig. 2*A* is not as yet understood, and it is conceivable that the circuit elements represent equivalent mechanical components such as mass, resistance and compliance. One alternative type of mechanism considered later (p. 408) which would involve electrical elements is a voltage- and time-dependent membrane conductance. The small signal behaviour of such a voltage-sensitive conductance can be represented by a resonant circuit involving two resistors and an inductance (Hodgkin & Huxley, 1952; Mauro, Conti, Dodge & Schor, 1970; Detwiler, Hodgkin & McNaughton, 1980). If the membrane capacity is included, the equivalent circuit for this kind of mechanism would be that shown in Fig. 2*B*. The differential equation for the circuit is:

$$\dddot{V}+\gamma\ddot{V}+\omega_0^2\dot{V} = \frac{IR_1}{LC}+\frac{1}{C}\dot{I}, \tag{17}$$

where

$$\gamma = \frac{R_1}{L}+\frac{1}{R_2 C}$$

$$\omega_0^2 = \frac{1}{LC}\left(1+\frac{R_1}{R_2}\right).$$

The circuit behaves very similarly to that in Fig. 2*A*, which has been considered already; the main effect of the extra resistance, R_2, is to produce an additional damping. It may be shown that if R_2 is large compared to R_1 the quality factor, Q', of the circuit is approximately related to the Q of the circuit in Fig. 2*A* by

$$\frac{1}{Q'} = \frac{1}{Q}+\frac{1}{R_2}\sqrt{\frac{L}{C}}, \tag{18}$$

with $R_1 = R$.

RESULTS

Oscillatory responses to current steps

When a rectangular current is injected into the hair cell through the recording electrode the cell potential undergoes a damped oscillation at the beginning and end of the current step. This section deals with the properties of these oscillatory responses and their relationship to the tuning of the receptor potential to sound stimuli.

The basic phenomenon is illustrated in Figs. 4, 5 and 7, which show the effects of injecting constant current steps into several hair cells. When the magnitude of the injected current was small enough to produce a steady-state deflexion of the membrane potential from its resting value by less than 5 mV the damped oscillation occurring during the current pulse had approximately the same frequency and time

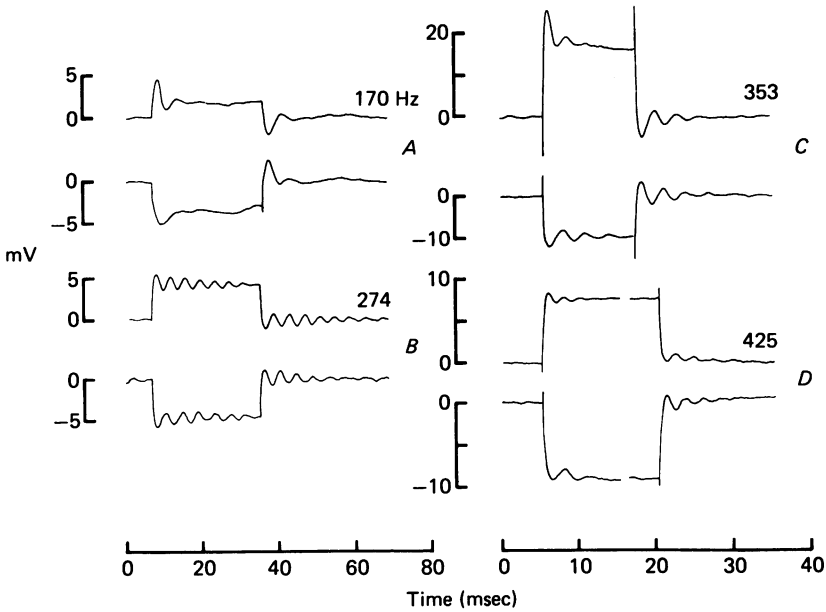

Fig. 4. Examples of oscillations in the hair-cell membrane potential in response to injection of current steps into four hair cells with different characteristic acoustic frequencies. The characteristic frequency of the cell is given beside each pair of traces. The current was injected down the recording electrode, and the voltage drop across the electrode resistance balanced out with a bridge circuit. For each trace, a number of responses were averaged in order to reduce the basal noise in the hair-cell potential (see Crawford & Fettiplace, 1980*a*); the variance of this voltage noise was of the order of 1 mV^2. All voltages given relative to the resting potential. The magnitudes of the depolarizing (+) and hyperpolarizing (−) currents, the resting potential and the number of responses averaged were: *A*, ±0·08 nA, −51 mV, 256; *B*, ±0·024 nA, −54 mV, 128; *C*, +0·37 nA, −0·15 nA, −48 mV, 32; *D*, ±0·18 nA, −46 mV, 32. Note that the frequency of the oscillations changes with the characteristic frequency of the cell, the time scale for *A* and *B* being different from that for *C* and *D*.

constant of decay as that occurring at the end of the current pulse, and these quantities were independent of the polarity of the applied current. Several examples of small current responses are illustrated in Fig. 4. In the cell shown in Fig. 4*B*, where the oscillations are particularly pronounced, a current of −24 pA produced ringing at 258 Hz during the current step and 261 Hz at its termination. A current of +24 pA caused an oscillation at 290 Hz during the depolarizing current and an oscillation at 265 Hz when the current ceased to flow.

Initially we were interested in determining whether the frequency of oscillations to small current steps varied systematically from hair cell to hair cell and whether any such variation was correlated with the frequencies to which hair cells were

acoustically tuned. In eight cells the frequencies of the electrical oscillations (f_e) were measured and then for each cell the characteristic acoustic frequency was determined according to the methods described previously (Crawford & Fettiplace, 1980*a*). Briefly, a tone was swept from 10 Hz to 3 kHz at various constant intensities and the modulus of the receptor potential measured. At low sound-pressure levels the

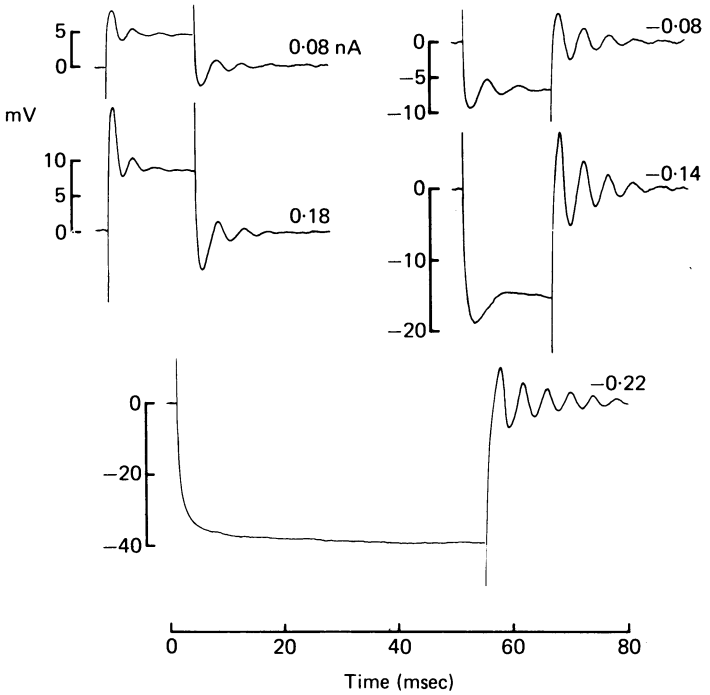

Fig. 5. Averaged responses of a hair cell to injection of rectangular current pulses of duration 15·4 msec (top four traces) or 54 msec (bottom trace). Current magnitude given in nA beside each trace, and for each current sixty-four responses have been averaged. Voltage drop across electrode resistance balanced out with bridge circuit. Note that the frequency of the 'on' oscillations varies with current strength and that the oscillations vanish for large hyperpolarizing currents (bottom trace). Voltages given with respect to resting potential, −54 mV; Acoustic characteristic frequency at this point in recording 237 Hz; 21·5 °C.

iso-intensity response curves are superimposable if scaled by a factor proportional to the sound pressure used, and all show a sharp maximum. The frequency to which the cell is maximally sensitive in its linear range is designated the characteristic acoustic frequency (see Crawford & Fettiplace, 1980*a*).

Fig. 6 shows a graph of the characteristic electrical frequency *versus* the characteristic acoustic frequency for the eight cells. All points lie close to a line with a slope of 1·0 on linear co-ordinates indicating that the electrical oscillations for small current pulses occur at the characteristic acoustic frequency of the cell, and that different hair cells have different electrical frequencies ranging from 100 to 425 Hz in the examples illustrated. The results of the measurements are presented in Table 1.

Larger current steps still produced voltage oscillations, but a frequency non-linearity

became obvious in all cells examined. Figs. 5 and 7 illustrate the potential responses to currents of different magnitude and polarity in two cells. Large depolarizing currents increased and large hyperpolarizing currents reduced the frequency of the oscillations during the current pulse. Thus in Fig. 7 a current of −0·32 nA caused an initial ringing at 240 Hz and a terminal oscillation of 350 Hz. A current of +0·37 nA produced an oscillation at 406 Hz at current 'on' and at 343 Hz at current 'off'. The

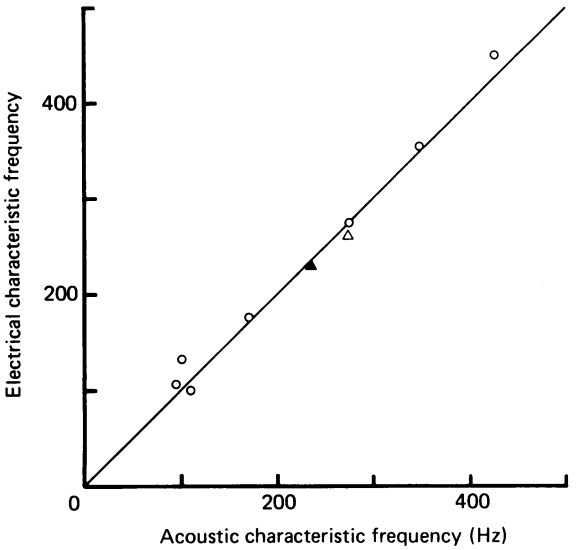

Fig. 6. Correlation between acoustic and electrical characteristic frequencies for eight different cells. Ordinate is the frequency of the voltage oscillations at current 'off' for small currents. Abscissa is the acoustic characteristic frequency derived from the linear tuning curve and from the terminal oscillations to untapered tone bursts. The line drawn through the origin has a slope of 1·0. The filled and open triangles are from measurements on the same cell at different times during the recording.

characteristic acoustic frequency of this cell was 353 Hz. We consistently observed that the oscillations following current pulses were largely independent of the magnitude or polarity of the currents which preceded them, but that oscillations occurring during the passage of current across the hair cell membrane were strongly dependent, both in terms of frequency and time course, on the current flowing.

The form of the responses illustrated in Figs. 4, 5 and 7 is reminiscent of the voltage produced when a constant current is delivered to the circuit, illustrated in Fig. 2*A*, which consists of a capacitor connected in parallel with a resistor and an inductance. In Fig. 7 the open circles superimposed upon the hair cell potential records have been calculated according to a slightly modified form of eqn. (15):

$$V'_u = IR_e + V_u(t) - V_u(t-T), \tag{19}$$

where V_u is the response of the parallel *LRC* circuit to a constant current step of magnitude I and is given by eqn. (13). R_e is an arbitrary constant representing the value of a resistance placed in series with the *LRC* circuit and needed to obtain the correct steady-state value of the hair cell potential during the current step. In the example of Fig. 7 R_e was about 60 MΩ.

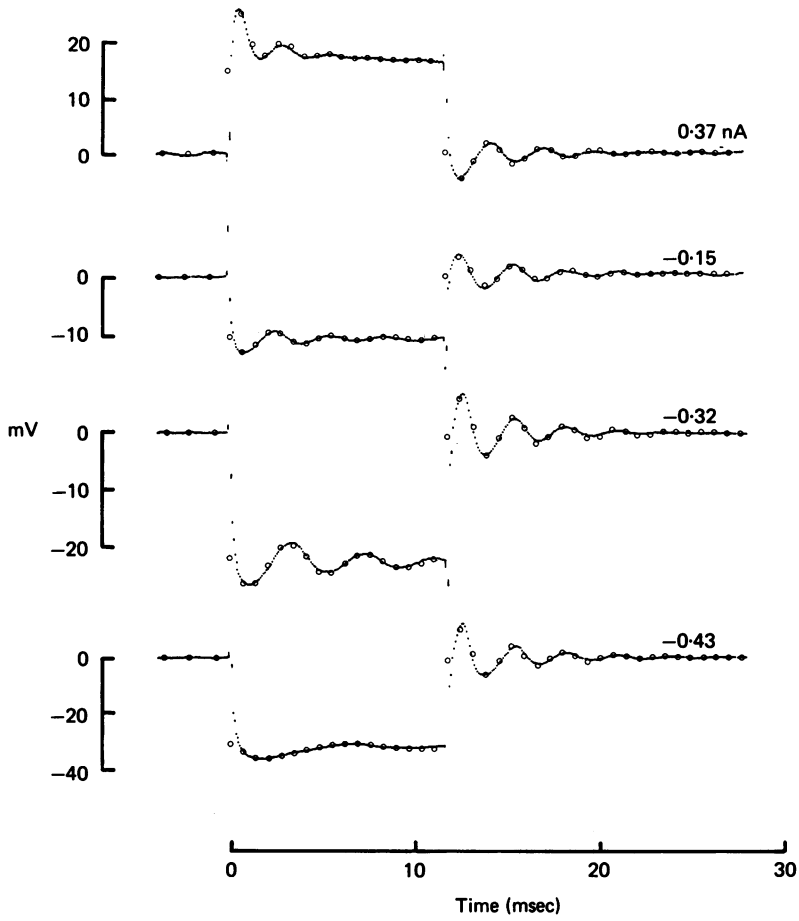

Fig. 7. Averaged membrane potential changes of a hair cell to injection of rectangular current pulses of duration 11·8 msec; current magnitude in nA given beside each trace, which is the average of sixty-four responses. Voltage drop across electrode resistance balanced out as well as possible with a bridge circuit. The open circles have been calculated using eqns. (13) and (19) in the text on the assumption that the hair cell behaves like an electrical resonator; the frequency, f_R, and time constant of decay, τ, of the oscillations and the resistance, R, were chosen empirically to best fit the responses, with different values for f_R and τ at current 'on' and current 'off'. The values used for the parameters were:

		On		Off	
I (nA)	R (MΩ)	f_R (Hz)	τ (msec)	f_R (Hz)	τ (msec)
+0·37	3·38	406	2·00	343	3·5
−0·15	2·67	322	4·00	359	4·0
−0·32	2·34	240	5·5	350	3·5
−0·43	3·72	121	4·95	363	3·5

Voltages are given with respect to the resting potential, −48 mV; acoustic characteristic frequency 353 Hz; temperature 21 °C.

The need to include the series resistor R_e may simply arise from imbalance in the bridge, but other less trivial explanations are possible. For example, if each hair cell were electrically coupled to others of similar characteristic electrical frequency, the steady-state potential would be determined by the coupling resistance as well as by the equivalent resistors of the resonant circuit. We confirmed this behaviour in calculations of the step response of a network of coupled elements each similar to that

TABLE 1. Comparison of the acoustic tuning and electrical resonance in several hair cells

			Acoustic tuning characteristics		Electrical tuning characteristics			
Cell number	E_r (mV)	R_{max} (mV)	f_a (Hz)	Q_a	f_e (Hz)	τ (msec)	Q_e	Temp. (°C)
1	−50	34	86	2·91	108	13·95	4·73	22
2	−55	45	100	1·33	134	3·23	1·36	21
3	−50	32	111	1·66	101	5·45	1·73	24
4	−51	22	170	1·66	179	2·99	1·68	24
5*	(−54	—	237	6·28	233	4·50	3·29)	21·5
	(−54	34	274	9·00	263	13·3	11·00)	
6	−48	18	276	6·75	276	5·56	4·82	19·5
7	−48	36	353	4·83	358	4·00	4·50	21
8	−46	28	425	4·82	440	3·28	4·54	25

E_r, resting potential; R_{max}, maximum peak-to-peak response of cell; f_a, Q_a are acoustic characteristic frequency and quality factor, and are means derived from measurements of linear tuning curves and terminal oscillations of linear responses to tone bursts. f_e, electrical characteristic frequency obtained from voltage oscillations to small current steps; τ, time constant of decay of oscillations; Q_e electrical quality factor derived from f_e and τ.

* Two sets of data taken at different times during recording.

in Fig. 2*A*. When three to seven elements were coupled in a row through resistances whose values were equal to the resistance in the single element, the resonant frequency and damping of the single element would be correctly estimated to within experimental error from the initial voltage oscillations when injecting a current step at a point. The amplitude of the oscillations was however reduced relative to the steady d.c. level.

During the passage of large depolarizing currents the voltage oscillations occurred around a mean level that declined slowly with time. The relaxation can be described reasonably well (see Fig. 7 upper trace) by allowing R_e to decay exponentially with time to a slightly smaller value. In Fig. 7, for a current of +0·37 nA, the open circles were calculated by allowing R_e to relax from 60 MΩ at the beginning of the pulse to 40 MΩ with a time constant of 4 msec. It is not clear whether this effect represents a small time-dependent change in the electrode resistance or whether the conductance of the cell might undergo a slow increase with time.

The calculations used in generating the open circles in Fig. 7 assume that the cell behaves as a parallel resonant circuit whose resonant frequency (f_e) and damping factor (γ_e) are both instantaneous functions of the constant current injected. The points describe the oscillations quite well, but it is noticeable for times less than a millisecond at the beginning and the end of the current pulse that the records change more slowly than the simple resonant circuit predicts. Part of this discrepancy may

be due to the limited band width of our recording system, but it could also indicate that the constants assumed to vary instantaneously in the resonance equations actually reach their new values with a small delay.

Table 1 summarizes the measurements of electrical tuning derived from using eqn. (13) to fit the small current responses in eight cells. For each cell, the characteristic electrical frequency and electrical quality factor are tabulated together with the characteristic acoustic frequency and acoustic quality factor. For cells where linear current responses were not available, the electrical parameters have been taken from measurements of the voltage oscillations when the current was turned off, as these approximate the linear behaviour of the cell. The electrical quality factor can be calculated from the time constant ($\tau = 2/\gamma$) of decay of the electrical oscillations and their frequency (f_e) by combining eqns. (4) and (7) in the theory section:

$$Q_e = [(\pi f_e \tau)^2 + \tfrac{1}{4}]^{\frac{1}{2}}, \tag{20}$$

which, when Q_e is large, becomes

$$Q_e \simeq \pi f_e \tau. \tag{21}$$

The acoustic quality factor, Q_a, has been obtained in two different ways: firstly from measurements of the linear tuning curve using the following equation

$$Q_a = \frac{f_a}{f_1 - f_2}, \tag{22}$$

where f_a is the characteristic acoustic frequency to which the cell is maximally sensitive and f_1 and f_2 are the frequencies on either side of f_a at which the sensitivity has fallen to $1/\sqrt{2}$ of that at f_a; secondly, Q_a has been derived from the decay of the oscillations at the end of a response to a tone burst at a frequency close to f_a. The two methods have been shown to give similar values for the acoustic quality factor (Crawford & Fettiplace, 1980*a*).

There is excellent agreement between the sets of electrical and acoustic measurements given in Table 1, which leads us to believe that the tip of the tuning curve is contributed by the electrical resonance phenomenon.

We reported in a previous paper (Crawford & Fettiplace, 1980*a*) that the acoustic tuning of a hair cell often improved quite substantially soon after the beginning of a recording. Thus cell 5 in Table 1 was tuned to 237 Hz with an acoustic quality factor of 6·3 at the beginning of the recording, but later the characteristic frequency rose to 274 Hz and the acoustic quality factor increased to about 9·0. Small currents caused electrical oscillations at 233 Hz with a quality factor of 3·3 at the beginning of the experiment, while later the electrical characteristic frequency and quality factor had increased to 263 Hz and 11·0. Thus even when the tuning properties of a cell were non-stationary, good agreement existed between estimates of electrical and acoustic tuning. We therefore suspect that most of the improvement we see in the tuning of cells during our recordings represents the recovery of the electrical filter from the damage of the initial impalement.

A confirmation that the electrical resonance phenomenon has a direct action on acoustically generated currents comes from experiments where extrinsic current was injected during the presentation of sounds. Intense sounds presented well below the

characteristic frequency of a hair cell caused the receptor potential to assume the form of a rectangular wave with a damped oscillation imposed on the plateau (Fettiplace & Crawford, 1978). A detailed examination of the phenomenon of acoustic ringing will be deferred to the next paper (Crawford & Fettiplace, 1980*b*), but it is worth mentioning at this point that the frequency of the acoustic ringing can be altered

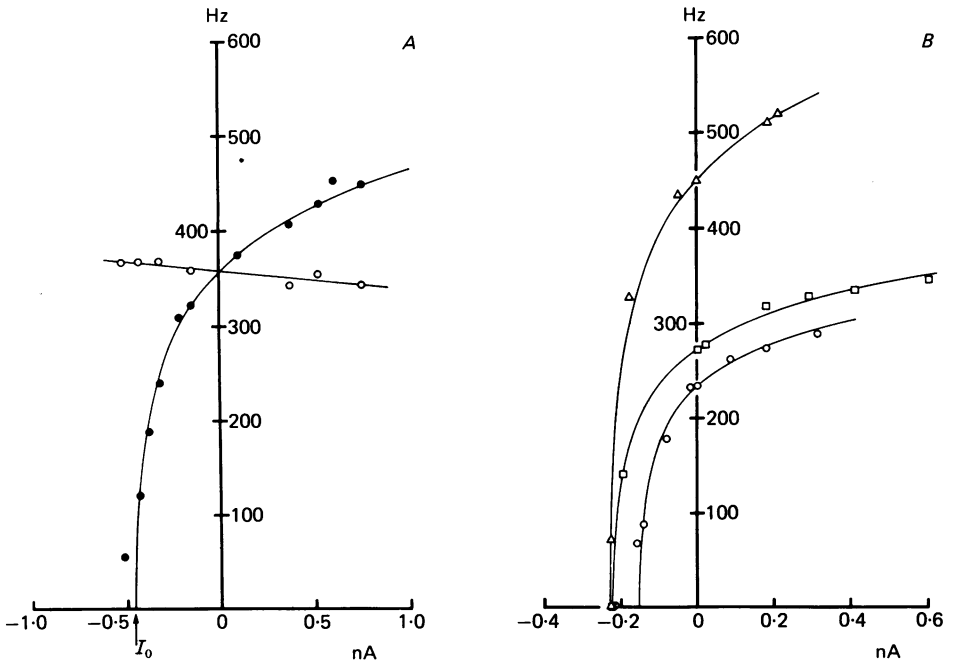

Fig. 8. Frequency of the voltage oscillations to rectangular currents as a function of current strength in four cells: *A*, ●, oscillations at current 'on'; ○, oscillations at current 'off'; results from cell of Fig. 7. *B*, oscillations at current 'on' for three other cells; acoustic characteristic frequency: △, 425 Hz; □, 276 Hz; ○, 237 Hz. Smooth curves for 'on' oscillations calculated using eqn. (23) in text with parameters given in Table 2. I_0 is defined in eqn. (23). The steady-state current-voltage curves for each of the cells showed a marked rectification, the conductance increasing with depolarization.

by the injection of standing currents into the cell. A hyperpolarizing current reduces, and a depolarizing current increases the acoustic ringing frequency, a result to be expected from the frequency non-linearity of the electrical filter. Interactions between extrinsic and intrinsic current of this sort provide direct evidence that the electrical resonance contributes to acoustic tuning.

Non-linearities in the electrical resonance for large current steps

By applying fitting procedures such as those given in Fig. 7 it was possible to examine how the frequency and time constant of decay of the electrical oscillations varied as a function of the injected current. Examples are given in Figs. 8 and 9 and further data are presented in Table 2. For the cell illustrated in Fig. 7, Fig. 8*A* shows changes in the ringing frequency as a function of the strength of the injected current. The ringing frequency during the pulse increased for depolarizing current, and with

increasing hyperpolarizing current the ringing frequency was reduced until eventually all oscillatory behaviour disappeared. Larger hyperpolarizing currents produced a monotonic hyperpolarization of the cell to a steady potential (see Fig. 5, −0·22 nA trace). The oscillations occurring at the end of the current pulse (open circles in Fig. 8*A*) changed little with the magnitude or polarity of the preceding current step, and any changes in the terminal ringing frequency that did occur tended to have a current dependence in the opposite direction to that seen for ringing during the current pulse.

TABLE 2. Constants used to fit the changes in electrical ringing with current strength

Cell number	E_r (mV)	f_e (Hz)	$\bar{f}$ (Hz)	μ (nA^{-1})	I_0 (nA)	K_1 (msec)	K_2 (nA^{-1})
1	−54	233	55·12	450	−0·15	4·29	4·26
2	−48	276	62·43	350	−0·22	5·77	2·25
3	−48	358	92·98	100	−0·46	3·42	1·3
4	−46	440	105·92	300	−0·23	3·28	5·08

E_r, resting potential; f_e, electrical characteristic frequency; columns 4–6 are parameters used to fit variation in electrical ringing frequency with current strength in eqn. (23), $f_R = \bar{f} \log_e (1+\mu(I-I_0))$; columns 7 and 8 are parameters used to fit variation in time constant, τ, of decay of oscillations with current strength in eqn. (24), $\tau = K_1 e^{-K_2 I}$.

Since for very small currents the initial and terminal ringing frequencies converge, the lines drawn through the points in Fig. 8*A* cross the zero-current axis together; this point of intersection may be used as the best estimate of the characteristic electrical frequency of a cell.

Plots of ringing frequency *versus* current strength are given for three other cells in Fig. 8*B*. The general forms of the plots are all quite similar and can be described by the empirical equations

$$\begin{aligned} f_R(I) &= \bar{f} \log_e (1+\mu(I-I_0)) \qquad I \geqslant I_0 \\ f_R(I) &= 0 \qquad\qquad\qquad\qquad\quad I < I_0, \end{aligned} \tag{23}$$

where f_R is the frequency of oscillations occurring during a current step of amplitude I, I_0 is the outward current just necessary to suppress the oscillations, and $\bar{f}$ and μ are constants for the cell with the dimensions of Hz and reciprocal current respectively. Eqn. (23) has been used to generate the smooth curves in Fig. 8 and the values of the constants used together with other electrical properties of the four cells are given in Table 2. An interesting conclusion of this analysis is that cells with different electrical characteristic frequencies have different values of the constant $\bar{f}$, which reflects the fact that the curves in Fig. 8 differ mainly by scaling on the ordinate; translation of the curves on the current axis does not allow them to be superimposed and it therefore seems unlikely that different cells have different electrical resonant frequencies by virtue of possessing either different resting potentials or shifted versions of the same voltage sensitivity.

Inspection of the records in Fig. 7 shows that the oscillation during a current step decays more slowly for negative current than it does for positive current, although the terminal oscillation which follows a current pulse relaxes in much the same way no matter what the magnitude or polarity of the preceding current. Fig. 9*A* shows,

for the cell illustrated in Fig. 7, measurements of τ, the time constant of decay of the oscillations as a function of current. For a simple resonant circuit the damping factor, γ, is given by $2/\tau$ (see eqn. (13)).

Measurements of τ were less reliable at large values of inward or outward current because the quality factor of the electrical resonance decreased as the membrane potential was displaced from its resting value and fewer oscillations were present from

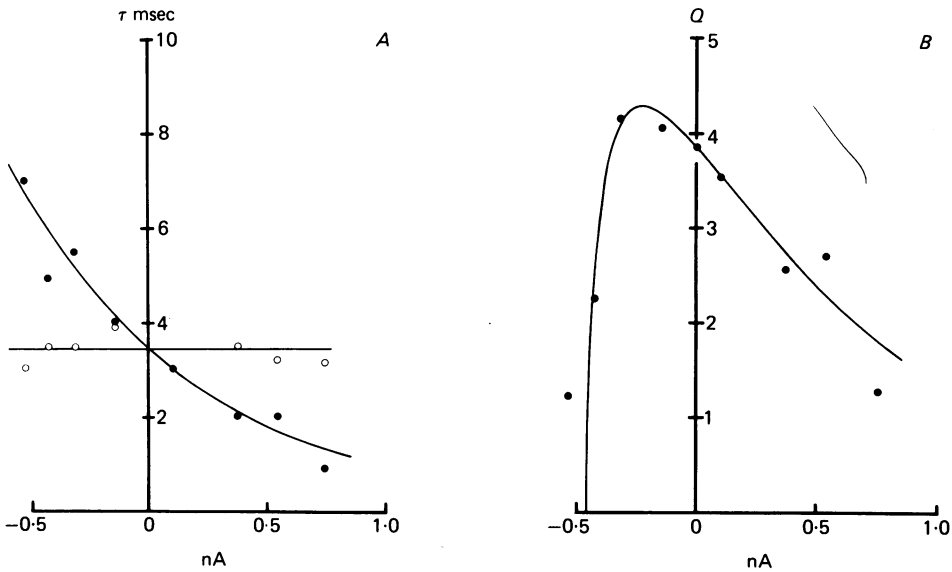

Fig. 9. Tuning of electrical resonance as a function of current strength for cell of Fig. 8*A*. *A*, time constant, τ, of decay of voltage oscillations at current 'on' (●) and current 'off' (○), plotted against current strength, outward currents positive. Curve through 'on' points calculated from eqn. (24). *B*, quality factor, Q_e, of electrical resonance derived from frequency (Fig. 8*A*) and decay time constant of 'on' oscillations using eqn. (20). Point on the ordinate axis is mean of 'off' values. Smooth curve has been calculated by combining the empirical expressions for f_e and τ as a function of current, using eqns. (20), (23) and (24). Other details for this cell are given in legends to Figs. 7 and 8*A*.

which to extract the time constant of decay. Nevertheless in all cells examined τ decreased monotonically with depolarizing current and increased monotonically with hyperpolarizing current.

The dependence of τ on current could be described empirically by the equation:

$$\tau(I) = K_1 e^{-K_2 I}. \tag{24}$$

This equation has been used to construct the smooth curve in Fig. 9*A* with $K_1 = 3{\cdot}417$ msec and $K_2 = 1{\cdot}3\,\text{nA}^{-1}$. A similar dependence of τ on current was seen in the three other cells, and the values of K_1 and K_2 required in eqn. (24) to fit these results are given in Table 2.

The quality factor of the electrical resonance (Q_e) at any level of current could be obtained from the time constant, τ, and the frequency, f_R, of the oscillations using eqn. (20). The dependence of the Q_e on the magnitude of the current step is given in Fig. 9*B*. For all cells examined, the quality factor had a maximum value close to

or slightly negative to the resting potential and declined if the cell were depolarized or hyperpolarized. Combining eqns. (23) and (24) above yields the empirical description of the dependence of Q_e on the current, which has been used to generate the smooth curve in Fig. 9*B*.

It is perhaps worth noting that a monotonic change with current in the value of any single component in the parallel *LRC* circuit cannot produce the observed dependence of the electrical quality factor on current strength.

Does current injection move the intracellular electrode?

One explanation that could account for the current-induced oscillations in the hair-cell potential would be that current injection causes the electrode to move the basilar membrane. The voltage oscillations might then be a consequence of a mechanical resonance in the basilar membrane motion. In an attempt to examine this possibility we have simultaneously recorded from single fibres in the auditory nerve while passing current through, or while displacing an intracellular electrode inserted into the basilar papilla at the level of, but not inside a hair cell.

The micro-electrode was mounted so that it could be moved perpendicularly to the basilar membrane (see Methods) and was also connected to the electrometer for passing current. For each nerve-fibre recording three types of measurement were made: acoustic stimulation yielded the characteristic frequency and sensitivity of the fibre; mechanical stimulation, using either step or sinusoidal displacements of the micro-electrode, allowed an estimate of its efficiency in moving the basilar membrane; and electrical stimulation, by passing current through the electrode, enabled us to assess whether there was any movement caused by the current.

We found in four preparations that the presence of a micropipette in the papilla did not significantly alter the sensitivity of single auditory nerve fibres to sound stimuli. Thus in one preparation the threshold for nerve fibres with characteristic frequencies from 120 to 660 Hz was $44{\cdot}5 \pm 7{\cdot}1$ dB s.p.l. (mean $\pm$ S.E.) before inserting the micropipette in the papilla and $50{\cdot}1 \pm 2{\cdot}6$ dB s.p.l. with the electrode in place. The effect of moving the papillar electrode is shown in Fig. 10*A* and *B*, which contain histograms of the timing of the impulses in two fibres in response to step displacements of the papillar electrode. The firing of each nerve fibre was modulated periodically at the beginning and end of the step, and resembles the pattern of discharge to a click. The interval between the peaks of the discharge was approximately equal to the reciprocal of the characteristic frequency of the fibre (see Fig. 10 and also Fig. 5 of Fettiplace & Crawford, 1980). At the beginning of the displacement, the firing rate initially increased if the pipette moved towards the scala vestibuli, whereas the basal discharge of the fibre initially decreased for a displacement away from the scala vestibuli. The initial change in the probability of firing at the end of a step was of the opposite polarity to that occurring at the beginning.

The magnitude of the step displacement necessary to produce a detectable change in the probability of firing was always large; the smallest step used was about 29 nm and the largest 250 nm, but most fibres could be stimulated with a step displacement of 50–60 nm.

Sinusoidal movements of the papillar electrode at a frequency close to the characteristic frequency of the fibre caused a discharge in which the impulses phase

locked to the cycles of the mechanical stimulus. The minimum amplitude of displacement necessary to produce an increase in the firing rate of about 20% was, in four preparations, 8·5, 1·6, 2·8 and 8·9 nm. No significant difference existed in the acoustic sensitivities between these preparations. In any one preparation there was

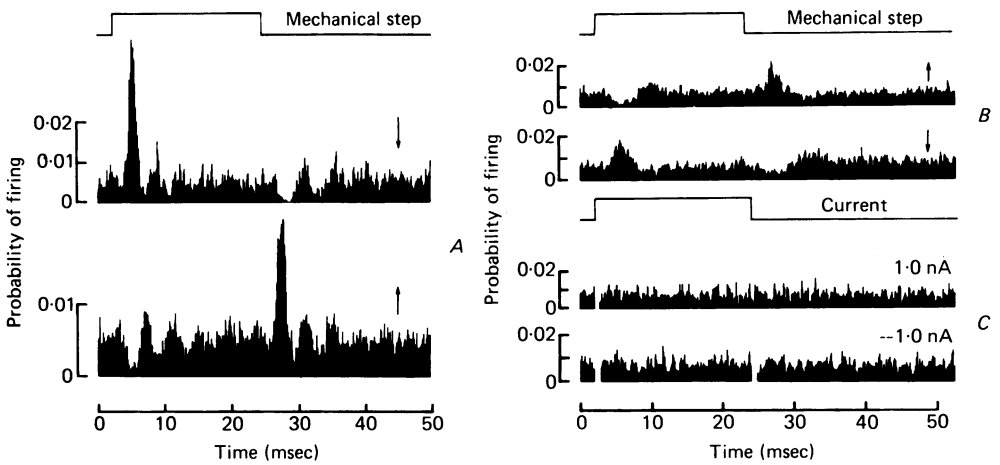

Fig. 10. Responses of two auditory nerve fibres to movements of the basilar membrane. For each fibre, histograms of the timing of the extracellularly recorded impulses were constructed from between 600 and 2700 stimulus presentations. Motion of the basilar membrane was produced by displacements of a high-resistance glass micropipette similar to those used for intracellular recording, which was inserted into the basilar papilla. The micropipette was fixed to the diaphragm of an earphone (see Methods). *A*, response of nerve fibre to 28·9 nm step displacements, toward scala media (↓) and away from scala media (↑). Characteristic frequency of cell, 275 Hz, acoustic threshold 59·5 dB re 20 μPa. *B*, response of nerve fibre to 51·4 nm step displacements, polarity indicated by arrows as in *A*; characteristic frequency of fibre 130 Hz, threshold 59·5 dB re 20 μPa. *C*, response of nerve fibre in *B* to current steps of $\pm$1·0 nA injected through papillar electrode. Capacitative artifacts at onset and offset of current, which have been omitted, are indicated by the gaps in the histograms.

little variation in the minimum amplitude of the sinusoidal displacement needed to fire individual fibres no matter what their characteristic frequency, and nearly all fibres were stimulated by a displacement of 20 nm peak-to-peak. The sensitivity to sinusoidal displacement was thus greater than to step displacement, but this is to be expected from the sharp frequency selectivity of the auditory nerve fibre and hair cell responses (see Crawford & Fettiplace, 1980*a*). The position of the papillar electrode along the cochlea was not critical in determining the threshold for mechanical stimulation, but the electrode had to be re-inserted into the papilla at intervals if the mechanical sensitivity were to be maintained at a high level, presumably because it tended to slip out of the papilla after prolonged movement.

In all fibres examined, current injection through the papillar electrode failed to cause any change in the auditory nerve discharge. Currents of up to $\pm$1 nA were used, these being considerably larger than the magnitude of the current required to elicit damped voltage oscillations in hair cells. An example of the negative result is illustrated in Fig. 10*C* for a fibre for which the mechanical response is also given.

The peri-stimulus histograms show no evidence of changes in the basal probability of firing. In ten fibres (characteristic frequencies 120–660 Hz) mechanical and electrical stimulation were investigated, and in all cases a clear mechanical response was present, yet currents failed to stimulate the fibre. We conclude that, for the current range used in our hair-cell experiments, the passage of current down the recording electrode does not produce gross displacements of the basilar membrane. We cannot, however, rule out the possibility that current injection while an electrode is inside a hair cell causes a movement confined to that region of the papilla.

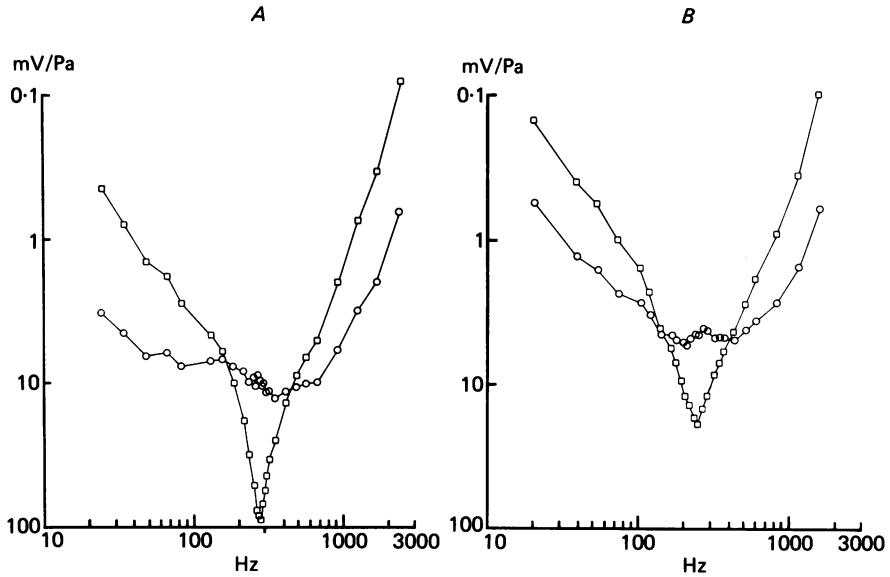

Fig. 11. Contribution of the electrical resonance to the acoustic tuning for two hair cells. For each cell, the linear tuning curve (squares) was derived from an iso-intensity frequency sweep which generated responses in the linear range (less than about 5 mV) at the characteristic frequency. The ordinate is a sensitivity, obtained by normalizing the r.m.s. voltage response to the sound pressure at each frequency. The residual filter (circles) was obtained by dividing the linear tuning curve by the normalized impedance of the electrical resonance ($A\omega_0 C/I$), calculated from eqn. (10) with the values of ω_0 and Q similar to those obtained from the responses to current steps. Values of f_e and Q used for the electrical resonance were *A*, 274 Hz, 9·0; *B*, 248 Hz, 4·0. The ordinate refers to both the linear and residual tuning curves, but the absolute voltage sensitivities for the residual tuning curves depend upon the normalization procedure adopted to describe the gain of the electrical resonator.

Contribution of the electrical resonance to acoustic tuning

The results presented in the first section of the paper and summarized in Table 1 demonstrated that in a number of hair cells there was a close correspondence between the characteristic frequency and quality factor of the electrical resonance and the characteristic frequency and quality factor of the cells tuning to sound stimuli. We concluded from these results that if the transducer current were subject to the same filtering operations as extrinsic current, the electrical resonance would account for the tip of the cell's acoustic tuning curve. In this section, we will examine the extent

to which the electrical resonance can explain the over-all shape of the linear tuning curves and try to estimate the additional filtering that must also be present.

In nine hair cells, linear tuning curves were measured as described in the Methods; examples for two cells are presented in Fig. 11 (squares). The linear tuning curve is the sensitivity of the cell (obtained by dividing the voltage response by the sound pressure) as a function of frequency when the cell is operating in its linear range.

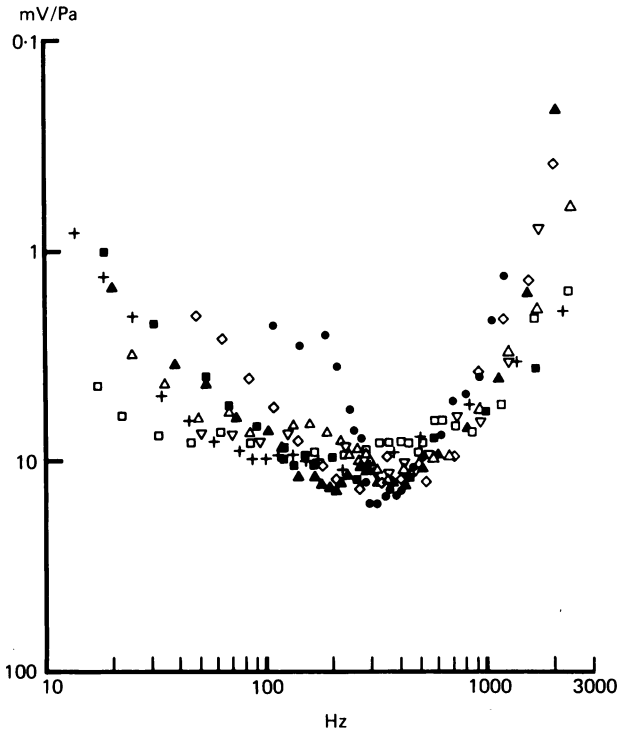

Fig. 12. Collected residual filter curves of eight hair cells. Each set of points was obtained by dividing the linear tuning curve by the normalized impedance of the electrical resonance ($A\omega_0 C/I$) calculated from eqn. (10). The ordinate is the sensitivity the cell would assume in the absence of the electrical resonance; since different cells had slightly different sensitivities, the measurements for a given cell have been multiplied by a scaling factor to superimpose the sets of points. The absolute sensitivities are given in Table 4. The values used for f_e and Q_e of the electrical resonance and the linear vertical scaling factors were: +, 106 Hz, 1·08, 0·32; ■, 181 Hz, 1·67, 17·9; ▲, 248 Hz, 4·0, 2·6; △, 274 Hz, 9·0, 1·0; ●, 305 Hz, 5·0, 0·87; ◇, 330 Hz, 4·0, 1·0; ▽, 425, 4·8, 3·3; □, 431, 6·0, 1·5. The values differ slightly from those obtained from the electrical ringing responses to current steps owing to small changes in the cell tuning during a recording. For cells ●, □, no electrical data was available and so values for f_e and Q_e are based upon measurements of tip of tuning curve.

For two linear independent filters in series the over-all gain at a given frequency is the product of the gains of the component filters, and the over-all phase shift introduced by the tuning mechanism is the sum of the phase shifts introduced by each of the two filters. Thus by dividing the linear tuning curve of a hair cell by the frequency response of the equivalent electrical circuit for that cell, the contribution of the electrical resonator to the over-all frequency selectivity can be estimated. This

procedure assumes (1) that the electrical resonance is independent of other filtering processes that are taking place and (2) that intrinsic currents generated by the transduction mechanism in the hair cell will develop across the cell membrane a voltage proportional to the impedance of the electrical resonator. The normalized membrane impedance $\left(\frac{A\omega_0 C}{I}\right)$ as a function of frequency has been calculated from eqn. (10) (Theory) using the characteristic electrical resonant frequency and quality factor obtained from the response to current steps. The normalized impedance, rather

TABLE 3. Values for the elements in the resonant circuit in a number of hair cells

f_e (Hz)	R (MΩ)	L (kH)	C (pF)
179	23·4	33·4	21·6
233	9·0	20·1	22·7
263	4·2	27·8	13·2
276	4·5	12·4	26·8
358	2·7	4·8	41·2
440	9·7	16·0	8·2

f_e, electrical characteristic frequency; R, resistance, L, inductance, C, capacitance in resonant circuit of Fig. 2A, derived from the fits to small current responses using eqns. (3), (4) and (13).

than the absolute impedance, was used because it allows the gain of the resonator to be specified solely in terms of ω_0 and Q, and does not explicitly involve the circuit parameters. Since the normalized impedance is dimensionless, it provides a measure of the relative gain of the resonator as a function of frequency. It should be pointed out, however, that the absolute gain has no significance as it depends upon the normalization procedure adopted (see p. 402).

The results of the division for two cells are illustrated in Fig. 11 (circles), where it can be seen that in both cases, most of the tip of the tuning curve has been removed by correction for the action of the electrical filter. The filter that remains after division we have called the residual tuning curve, and for the two cells this curve shows a decline in sensitivity at the extremes of the frequency range which is roughly proportional to the square of the frequency at high frequencies and to the frequency at low frequencies.

The residual tuning curve presumably reflects the action of frequency-selective mechanisms that precede the flow of current in a hair cell. The residual tuning curves for eight cells tuned to frequencies between 106 Hz and 431 Hz are illustrated in Fig. 12. For two of the cells, no electrical data were available and therefore the values of the electrical characteristic frequency and quality factor have been taken as being equal to those obtained from the tip of the tuning curve, by analogy with the measurements on the rest of the cells. Since different cells have slightly different absolute sensitivities the residual sensitivity for each of the cells in Fig. 12 has been scaled to superimpose the sets of points, which involves not more than a factor of ± 10 dB. The maximum residual sensitivity in mV/Pa for each cell before the scaling is given in Table 4.

Fig. 12 shows that all cells shared a common attenuation in sensitivity at high frequencies, which can roughly be described by a second order low-pass filter with

TABLE 4. Characteristics of residual filter after correction for electrical resonance

Cell number	Symbol	f_a (Hz)	Properties of residual modulus curves: Plateau sensitivity (mV/Pa)	Plateau sensitivity (nA/Pa)*	Limiting low-frequency slope (dB/decade)	Low-frequency corner (Hz)	Low-frequency corner based on a phase lead of 225° (Hz)	Low-frequency corner based on a phase lead of 270° (Hz)
1	+	100	32	0·45	33	58	—	49
2	■	170	0·65	0·014	27·5	118	—	128
3	▲	248	4·9	0·17	22	120	107	—
4	△	274	10	0·24	20	74	30	—
5	●	305	11·5	0·50	39	350	—	62
6	◇	353	13·8	1·26	24·7	210	160	—
7	▽	425	5·0	0·11	—	—	—	—
8	□	431	5·6	0·33	22·6	29	59	—

Symbols refer to residual modulus and phase diagrams in Figs. 12 and 16. f_a, characteristic acoustic frequency; columns 4–7 are from modulus curves after dividing by contribution of the electrical resonance; columns 8 and 9 are low-frequency phase leads after subtracting contribution of the electrical resonance. For a residual modulus curve with a limiting low-frequency slope of 20 dB/decade, the corner frequency should occur at a phase lead of 225°; if the slope is 40 dB/decade, the corresponding phase lead at the corner should be 270°.

* These values were obtained by multiplying the linear voltage sensitivity in the previous column by $\omega_0 C$, where C is the capacitance in the resonant circuit derived for each hair cell.

a corner frequency at 500–600 Hz. This kind of filter would also describe the performance of the middle ear in the turtle as measured recently by Moffat & Capranica (1978).

Different hair cells exhibited a somewhat variable low-frequency attenuation in sensitivity in their residual tuning curves. The low-frequency behaviour could be specified in terms of the corner frequency and limiting slope of the low-frequency attenuation, values of which are given in Table 4 for the various cells. For four of the cells the limiting slope was close to unity, with a corner frequency between about 30 Hz and 200 Hz. Thus in these cells the decline in sensitivity could be roughly described by the action of a simple first-order high-pass filter with a corner frequency that varied from cell to cell. For three of the other cells, the limiting slope was between one and two, with corner frequencies in the same range. For one cell no low-frequency cut was seen down to 50 Hz.

Unfortunately all the cells in Fig. 12, with the exception of those plotted as ● and ◇, were from different preparations, so we are not in a position to tell whether the variability in the lower corner frequency represents differences between preparations or whether each hair cell has a private high-pass filter, perhaps of mechanical origin. The latter explanation seems less likely, for there is no obvious correlation between the characteristic acoustic frequency and the lower corner frequency of the residual tuning curve (see Table 4).

The main conclusion from these measurements is that while the tip of the tuning curve can be accounted for by the action of the electrical resonance, there is also a rather broad band-pass filtering operation before transduction of the vibrations of the basilar membrane into electrical signals in the hair cell.

In performing the divisions, we have used the normalized impedance, $\left(\frac{A\omega_0 C}{\bar{I}}\right)$ (eqn. (10)) as a dimensionless variable describing the frequency selectivity of the electrical resonance since we have no direct measurements of the capacitance, C, in the circuit of Fig. 2*A*. In theory, C could be determined from the values for R, ω_0 and Q derived from the responses to small current pulses. As described on p. 391, there is some uncertainty in the absolute value of R, but if we assume that the need to include the series resistance, R_e, is due solely to incomplete compensation for the voltage drop in the electrode resistance and not to electrical coupling between hair cells, then the circuit parameters R, L and C can all be specified. Values of these parameters for a number of cells are presented in Table 3. It can be seen from Table 3 that the value of C does not appear to vary systematically with frequency, and the mean of the values given is 22·3 pF. The mean is very close to a direct estimate of 18 pF for the hair cell's membrane capacitance (Crawford & Fettiplace, 1980*b*). The latter value is based on measurements of the membrane time constant in a hair cell treated with tetraethylammonium bromide, which abolished the electrical resonance. It should be noted that the values of R in Table 3 represent, in this analysis, the input resistances of the hair cells; the mean of the values, which is 8·9 MΩ, is less than one tenth of that in the absence of the electrical resonance (Crawford & Fettiplace, 1980*b*).

With a value for the capacitance, C, it is possible to express the gain of the residual filter in terms of an absolute linear current sensitivity. The procedure for each cell involves multiplying the linear voltage sensitivity by the admittance, $\omega_0 C$. As an

example, consider the hair cell of Fig. 11*A*, for which the residual filter has a maximum sensitivity of 10 mV/Pa. Using a value for C of 13·2 pF (Table 3, row 3) and a characteristic frequency for the hair cell of 274 Hz would give a maximum linear current sensitivity of 0·24 nA/Pa; values for the other cells are given in Table 4. The significance of the linear current sensitivity is that it is independent of the resonant

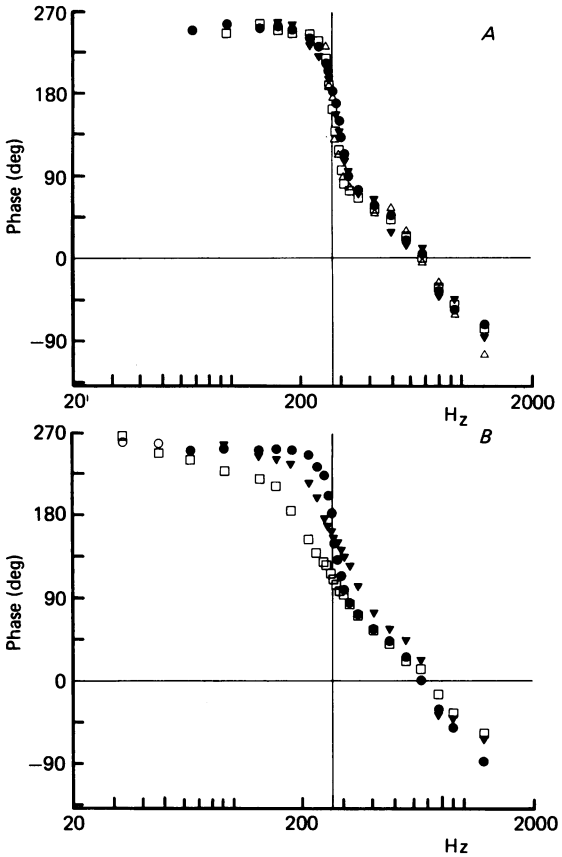

Fig. 13. The phase of the receptor potential in a hair cell as a function of frequency at various sound intensities. The ordinate is the phase of the hair cell voltage with respect to the sound pressure, with the convention that depolarizations and compressions are both positive quantities. Measurements were made on the responses to frequency sweeps at approximately constant intensity, using two phase-lock amplifiers to obtain the in-phase and quadrature components of the signal as described in Methods. Sound pressures in dB re 20 μPa were: *A*, ● 71 dB, ▼ 61 dB, △ 51 dB, □ 71 dB (run 2); *B*, ● mean of 51 to 71 dB values in *A*, ▼ 91 dB, □ 101 dB, ○ 81 dB; the rest of 81 dB points were indistinguishable from the mean curve. The measurements are uncorrected for the phase contributions of the sound measuring and the recording system. The corrections for this cell are given in Fig. 1*A*, *B* (curve c). The corrected invariant phase diagram for this cell is shown in Fig. 15*A*. Characteristic frequency = 274 Hz; Q = 9·0.

frequency, ω_0, and should be a direct measure of the sensitivity of the transduction mechanism. Excluding cell 2, which had a rather small maximum response amplitude, the mean current sensitivity from the values in Table 4 was 0·44 nA/Pa.

The phase of the receptor potential

In this section, we shall describe the phase behaviour of the cochlear mechanisms between the pressure wave at the tympanum and the receptor potential in the hair cell, and in the next section assess the contribution of the electrical resonance to this phase characteristic.

The phase angle was measured as a function of frequency at various constant sound pressure levels as described in the Methods. Fig. 13*A* shows the phase behaviour of the receptor potential in one hair cell for tones swept at intensities of 51 dB, 61 dB and 71 dB s.p.l. At 51 dB, the peak-to-peak response of the hair cell at its characteristic frequency was about 2 mV, which was still in the linear range. At all frequencies the phase was independent of intensity to within experimental error ($\pm 15°$); at low frequencies, the phase angle approached a lead of about 270°, then as the frequency was increased the phase underwent an abrupt lag of about 180° around the characteristic frequency of the cell (274 Hz) and showed a progressive lag at higher frequencies. We shall describe the phase characteristic as being invariant if it was obtained under conditions where the phase angle was independent of intensity at all frequencies.

At higher sound-pressure levels, the phase characteristics no longer remained invariant, as is shown in Fig. 13*B*. It can be seen that for iso-intensity sweeps at 91 and 101 dB s.p.l., the phase decline around the characteristic frequency was less steep than at lower intensities. The changes in phase angle with intensity were always more pronounced below the characteristic frequency, where the phase angle lead at high intensities was smaller than in the invariant phase diagram. This kind of behaviour could be produced by a non-linear filter whose damping factor changed with the input level.

Invariant phase diagrams for five other cells are shown in Fig. 14 in descending order of characteristic frequency. Each of the characteristics was obtained at a sound pressure where the response of the cell was within its linear range. The results have been staggered on the ordinate but the absolute phase lead of 180° is indicated for each cell together with an incremental phase-angle calibration. Note that all cells have an invariant phase diagram of similar form but that the inflexion in the phase angle around the characteristic frequency shifts to lower frequencies as the characteristic frequency decreases. It is also evident that the rate of change of phase around the characteristic frequency is related to the acoustic quality factor of the cell. Thus in Fig. 13*A* the hair cell had a quality factor of about 9 and there was an abrupt phase change around its characteristic frequency (274 Hz) while the lowest cell in Fig. 14 had a quality factor of about 1·7 and a very modest rate of phase change around its characteristic frequency (170 Hz).

Contribution of the electrical resonance to the phase diagram

In nine cells invariant phase diagrams were obtained together with measurements of the electrical quality factor and the electrical resonant frequency. The phase shift introduced by the electrical resonance phenomenon can be calculated according to eqn. (11) (Theory) whose form is illustrated in Fig. 3*B* for three values of the quality factor. In each of the nine cells the phase angle due to the electrical resonance was

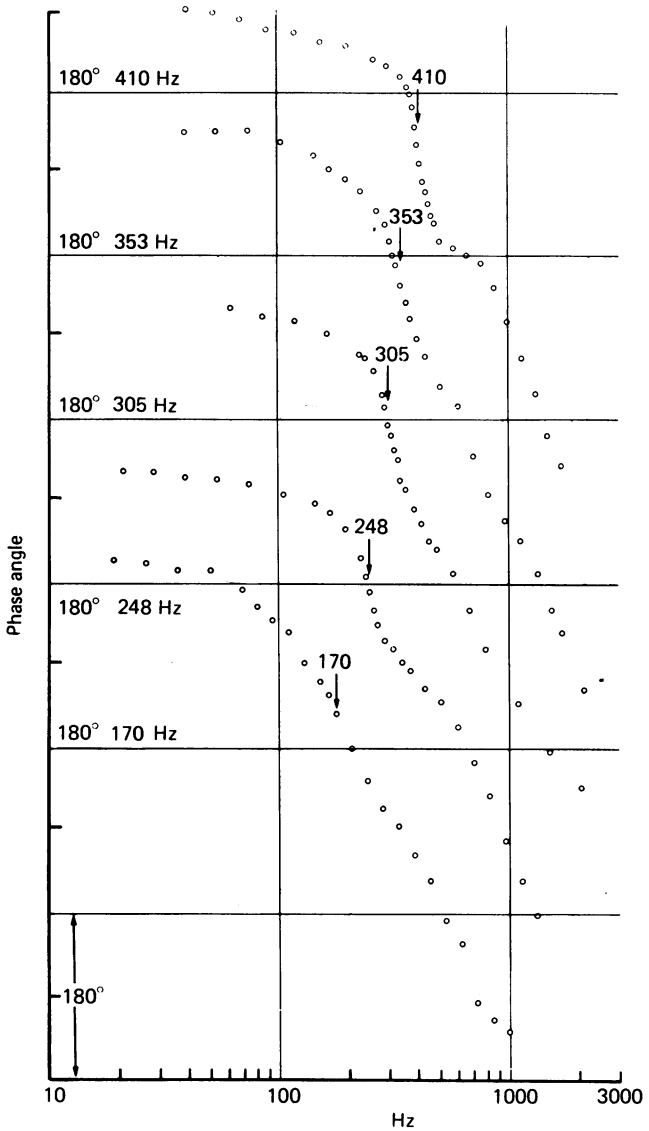

Fig. 14. Invariant phase characteristic for five hair cells. For each set of points, the position on the ordinate corresponding to 180° phase lead is marked along with the characteristic frequency of the cell. Measurements were taken from low-intensity frequency sweeps at which the phase was independent of sound pressure, with the phase convention as in Fig. 13. Note that there is an abrupt phase lag close to the characteristic frequency of the cell, the position of which on the abscissa is indicated by the arrow. All measurements have been corrected for the sound measuring and the recording systems. Quality factors of linear tuning curves were: 410 Hz, 6·0; 353 Hz, 4·8; 305 Hz, 5·0; 248 Hz, 4·0; 170 Hz, 1·66.

subtracted algebraically from the invariant phase diagram to produce a new phase plot which will be referred to as the residual phase characteristic.

Examples of residual phase characteristics for two cells are given in Fig. 15 together with the invariant phase diagram before subtraction. The two cells have been chosen because they have very different quality factors; in Fig. 15*A* Q was 1·07 and the resonant frequency was 134 Hz, while the cell of Fig. 13*B* had a quality factor of

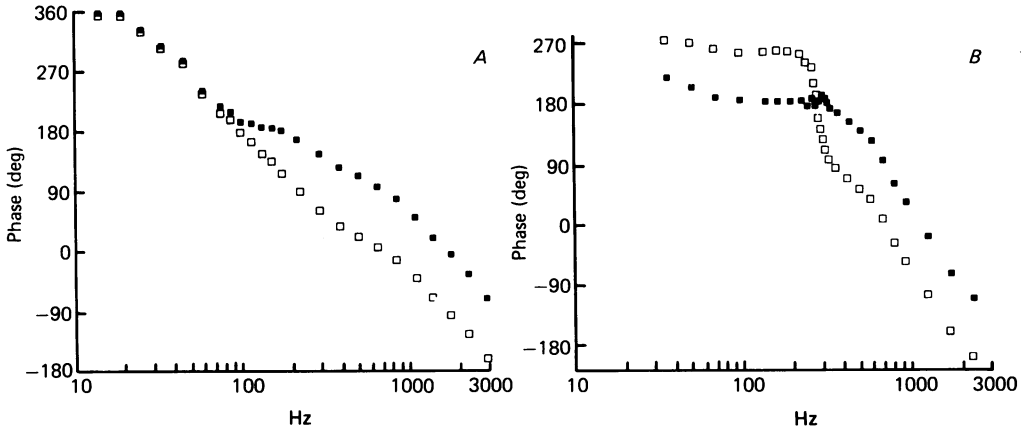

Fig. 15. Contribution of the electrical resonance to the linear phase behaviour of the hair cells. For each cell, the invariant phase characteristic (open symbols) has been corrected by subtraction of the expected contribution of the electrical resonance (calculated using eqn. (11)) giving the residual phase (filled symbols). Values of f_e and Q_e assumed for the electrical resonance were: *A*, 134 Hz, 1·07; *B*, 274 Hz, 9·0. Note that the residual phase exhibits a flat region of 180° lead around the characteristic frequency of the cell. Phase conventions as in Fig. 13; all measurements corrected for sound measuring and recording systems. The residual modulus for cell in *A* is denoted by + in Fig. 12; the residual modulus for cell in *B* is shown in Fig. 11*A*.

9·0 and a resonant frequency of 274 Hz. Despite these differences, the residual phase characteristics for the two cells show a number of features in common. Both give a phase lead of about 180° at the characteristic frequency. This result was found to be the case for all but one of the cells examined and is consistent with the conclusion given in Crawford & Fettiplace (1980*a*) that the polarity of the electromechanical transduction mechanism is such that the hair cells depolarize for displacements of the basilar membrane towards the scala vestibuli. This conclusion was previously based on the fact that in response to a click the hair-cell membrane potential undergoes a damped oscillation whose initial polarity is depolarizing for a rarefaction click and hyperpolarizing if the click is a condensation. Since, for the phase measurements described here, the convention used for defining the phase angle of the receptor potential was that compressions and depolarizations were considered to be positive, a phase lead of 180° indicates that the hair cell depolarizes for rarefactions.

The collected residual phase characteristics for seven cells are shown in Fig. 16. For each of the cells, it can be seen that the sudden phase inflexion around the characteristic frequency has been removed, and all exhibit a common phase behaviour

at frequencies above about 300 Hz. As the frequency decreases below this value the residual phase angle is found to remain at 180° lead for a variable frequency interval after which the lead increases, in different cells approaching leads of between 270° and 360°. This variable low frequency behaviour is consistent with the variable

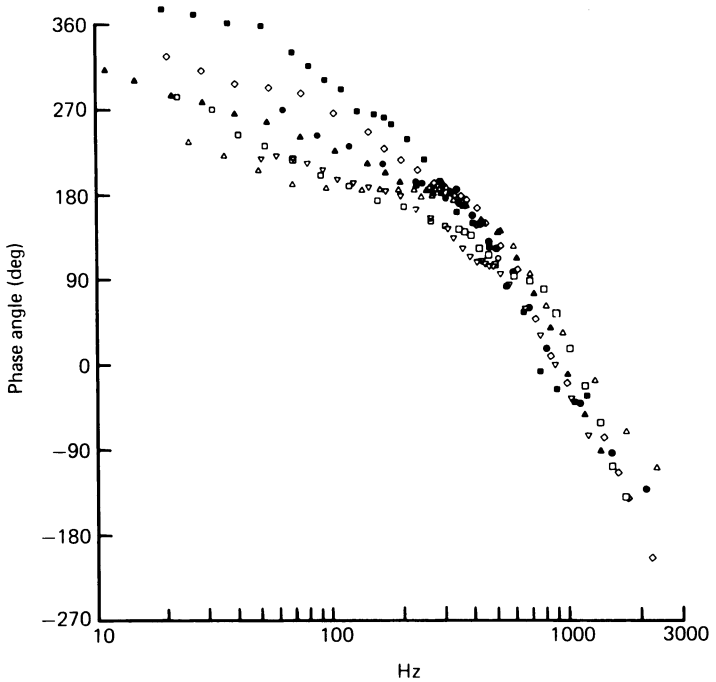

Fig. 16. Residual phase diagrams for seven hair cells. Each set of points obtained by subtraction of the expected contribution of the electrical resonance from the invariant phase curve for each cell. Values used for f_e and Q of the electrical resonance were: ■ 170 Hz, 1·66; ▲ 248 Hz, 4·0; △ 274 Hz, 9·0; ● 305 Hz, 5·0; ◇ 330 Hz, 4·0; □ 410 Hz, 6·0; ▽ 425 Hz, 4·8. The symbols used for each cell are the same as those in modulus curves, Fig. 12. Phase conventions as for Fig. 13. Note that the points from all cells superimpose at frequencies above about 300 Hz. Details of low-frequency phase lead for each cell are given in Table 4.

decline in sensitivity with decreasing frequency seen in the residual tuning curves (Fig. 12). The low-frequency phase behaviour for each of the cells is documented in Table 4. If the sensitivity of the residual modulus curve declines with a slope of unity at low frequency, the residual phase characteristic should asymptote to a lead of 90° in excess of the 180° at the characteristic frequency on the assumption that the residual filter behaves as a minimum phase filter. The corner frequency of the first-order high-pass filter should then occur at a lead of 225°. The results in Table 4 show a reasonable agreement between the corner frequencies obtained from the residual modulus and phase characteristics, and reinforce the idea that there is no correlation between the corner frequency and the characteristic frequency of the cell's tuning curve.

The phase results from one hair cell were anomalous, and are not included in Fig. 16. The cell (no. 1 in Table 1) was tuned to 86 Hz, which was the lowest characteristic acoustic frequency in our measurements, and reasonable agreement existed between electrical and acoustic tuning (see Table 1). The form of the invariant phase diagram was similar to that seen with other cells, but it was peculiar in showing a low-frequency phase asymptote of about 450°. After subtraction of the phase shift introduced by the electrical resonance the phase angle at the characteristic frequency was about 300°, not 180° as in other cells. The over-all phase diagram behaved as though an extra lead of about 90° had been introduced at all frequencies, but since this cell was also rather insensitive to sound we are reluctant to place any definite interpretation on the results.

We conclude from the phase subtractions: (1) that the electrical resonance contributes almost all of the sudden phase change seen around the characteristic frequency of the cell; (2) that some process, probably the middle ear, introduces a progressive phase lag common to all cells in the receptor potential above about 300 Hz.

DISCUSSION

This paper describes evidence for an electrical tuning mechanism which operates in the cochlear hair cells of the turtle. The mechanism, which would seem to account for most of the frequency selectivity of this animal, can be described in terms of a simple resonant circuit.

The first suggestion that electrical processes were involved in frequency selectivity of the cochlea was made by Gold (1948) in what was essentially an electromechanical feed-back model (discussed further in Wilson, 1977). Interest in electrical tuning processes has revived recently with the experiments of Hopkins (1976) on the electroreceptors of *Gymnotid* fish. Single nerve fibres from the tuberous electroreceptor cells, thought to be derived from hair cells of the acoustico-lateralis system (Szabo, 1974), are sharply tuned in each of the animals. The range of nerve fibre optimal frequencies observed by Hopkins (1976) in the electroreceptors of the three *Gymnotid* species was 50 Hz–1·2 kHz (25 °C), which spans the range of characteristic frequencies observed in the turtle cochlea. The tuning of the electroreceptors was anticipated in the observations by Bennett (1967) that a rectangular current pulse applied across the electroreceptor epithelium caused the receptors to generate damped oscillatory currents at the onset and offset of the pulse. The similarity of these observations to the results reported here may indicate that a common mechanism operates in tuned electroreceptors and in turtle hair cells.

The basis of the electrical resonance

There are two classes of hypothesis that might explain the physical basis of the electrical resonance seen in the hair cell. The first group would be electromechanical systems of the type suggested by Gold (1948). Since we have no evidence for a mechanical element in the resonance it does not seem fruitful at this stage to discuss this hypothesis further. An alternative hypothesis arises by analogy with the behaviour of voltage- and time-dependent membrane conductances described first in nerve by Hodgkin & Huxley (1952) and capable of producing the phenomenological inductance required to account for our results (Hodgkin & Huxley, 1952; Mauro *et al.* 1970; Detwiler *et al.* 1980). The equivalent circuit for small perturbations to a single voltage- and time-dependent conductance has been given in the Theory section (Fig.

2*B*) but, for a conductance turned on by depolarization, holds only if the membrane potential is positive to the reversal potential of the ionic current; for potentials negative to the reversal potential the inductance in the equivalent circuit is replaced by a capacitor (see Mauro *et al.* 1970; Detwiler *et al.* 1980). The behaviour arises because the ionic current flowing as a result of the conductance change reinforces rather than opposes the applied potential when the potential is negative to the reversal potential and results in an abolition of the membrane's oscillatory properties. In our experiments, the resonant behaviour disappears when the hair cell is hyperpolarized to about −80 mV, which suggests that a voltage-sensitive potassium conductance in the basal membrane of the hair cell might be involved in generating the resonance. The voltage-sensitive potassium conductance system in the squid axon is not normally much more than critically damped, and the hair-cell resonators have damping factors closer to that seen in nerve in low calcium solutions with both sodium and potassium conductances contributing (Huxley, 1959). This would argue that more than one type of voltage-sensitive conductance may be necessary to achieve the desired sharpness of resonance seen in the hair cells.

Injection of extrinsic current into a hair cell reveals two non-linearities: the damping factor and the resonant frequency both depend on the magnitude and polarity of the current injected. Our results do not allow us to distinguish whether these non-linear properties are current- or voltage-controlled, and we have expressed them in Figs. 8 and 9 as a function of the injected current merely to avoid the uncertainties in the bridge balance. It may eventually turn out that the resonator is voltage-controlled (as in the conductance hypothesis) and it should be pointed out that the precise form of the curves in Figs. 8 and 9 would then be modified. Steady-state current–voltage curves in all hair cells in which we have been able to achieve reliable bridge balance show a pronounced rectification such that the conductance increased markedly for depolarization, so that re-plotting the curves in Figs. 8 and 9 with membrane potential as the abscissa yields a more linear relationship for f_e or τ_e as a function of voltage than it does for current. Qualitatively at least, these non-linearities are known properties of the voltage-sensitive conductances. Thus, for example, the resonant frequency of the squid axon, which is about 120 Hz at the resting potential at 18·5 °C (Huxley, 1959; Mauro *et al.* 1970) changes with potential in the same manner as does the resonant frequency of the hair cell (Mauro *et al.* 1970; Conti, 1970).

A major difficulty in the conductance hypothesis is how to explain that the electrical resonant frequency of each hair cell changes systematically along the basilar membrane. In principle a variation could be achieved by changing the density of conducting channels from cell to cell (see for example the effect of altering $\bar{G}_K$ and $\bar{G}_{Na}$ in the treatment of Mauro *et al.* (1970)) or by altering the cell capacitance (for example by changing the dimensions of the hair cells) systematically along the cochlea. But in the absence of any direct evidence that the necessary conductances actually exist in the hair-cell membrane it seems premature to pursue the explanation further.

Consequences of non-linear resonance

In a previous paper (Fettiplace & Crawford, 1978) we reported that the relationship between the amplitude of the receptor potential and the sound pressure was a

monotonic saturating fraction whose maximum amplitude and half-saturation sound pressure depended on the frequency of stimulation: tones presented above and below the characteristic frequency caused the receptor potential to saturate at a lower amplitude and with a higher half-saturation sound pressure than at the characteristic frequency. It was noted that this effect was a property of two linear filters separated by an instantaneous compressive non-linearity of the type discussed by Pfeiffer (1970), Duifhuis (1976) and others. The present results provide independent evidence for this explanation; the second filter we would identify with the electrical resonator possessed by each hair cell and the first filter by a rather broad filter shared by all hair cells. The high-frequency portion of the initial filter is consistent with the performance of the middle ear in *Pseudemys* as reported by Moffat & Capranica (1978); it is conceivable that the low-frequency portion of the first filter reflects the action of the helicotrema. Our estimate of the frequency selectivity of processes preceding current flow in the hair cells (see Fig. 12) indicates that the basilar membrane motion confers little frequency selectivity in *Pseudemys*. A similar conclusion has been reached by Weiss *et al.* (1978) who directly measured the vibration of the basilar membrane in the alligator lizard, *Gerrhonotus multicarinatus*. While the latter measurements are on a different species, the dimensions and shape of the basilar membrane in the alligator lizard are so similar to those of the turtle that the comparison seems acceptable, even though there are major differences in the structure of the basilar papilla and distribution of the tectorial membrane between the two species.

We noted previously that in the simplest form of the band-pass non-linearity it is possible to extract the form of the two linear filters from the multiplying factors needed to scale the fundamental response *vs.* pressure functions on to a common curve (Fettiplace & Crawford, 1978). The method relies heavily on the values of the fundamental of the receptor potential obtained at high intensities and hence on the linearity of the filters at high intensity. The method of filter extraction presented here contains the assumptions that the filters are independent and that intrinsic and extrinsic currents flowing across the hair-cell membrane produce similar voltage wave forms, and allow the frequency and phase responses of the filters to be extracted using only low-level stimuli where the frequency selective processes are linear. At higher levels the electrical resonance behaves as though it were more damped, not only because the quality factor actually decreases but also because, for sinusoidal stimuli, the resonant frequency will oscillate around a mean position so that the frequency response averaged over a whole cycle will be broader and the average phase transition around the mean resonant frequency less rapid. Filter assessment according to the band-pass non-linearity treatment may therefore underestimate the gain of the second filter and over-estimate the gain of the first filter when the receptor potential is largest. Thus in Fig. 4*A* of Fettiplace & Crawford (1978) the small bump in the frequency response of the first filter close to the characteristic frequency of the cell is almost certainly spurious, and the method leads to the erroneous conclusion that the first filter is different for different hair cells.

We are especially indebted to Dr P. A. McNaughton for making a number of helpful suggestions during the course of the work. We also thank him, Dr J. G. Robson and Professor A. L. Hodgkin

for commenting on the manuscript. We acknowledge the support of the Medical Research Council and a grant from the Elmore Trust to R. F.

REFERENCES

BENNETT, M. V. L. (1967). Mechanisms of electroreception. In *Lateral Line Detectors*, ed. CAHN, P., pp. 313–393. Bloomington: University of Indiana Press.

COLBURN, T. R. & SCHWARTZ, E. A. (1972). Linear voltage control of current passed through a micropipette with variable resistance. *Med. biol. Engng* **10**, 504–509.

CONTI, F. (1970). Nerve membrane electrical characteristics near the resting state. *Biophysik* **6**, 257–270.

CRAWFORD, A. C. & FETTIPLACE, R. (1978). Ringing responses in cochlear hair cells of the turtle. *J. Physiol.* **284**, 120–122*P*.

CRAWFORD, A. C. & FETTIPLACE, R. (1980*a*). The frequency selectivity of auditory nerve fibres and hair cells in the cochlea of the turtle. *J. Physiol.* **306**, 79–125.

CRAWFORD, A. C. & FETTIPLACE, R. (1980*b*). Non-linearities in the responses of turtle hair cells. *J. Physiol.* (submitted).

DETWILER, P. B., HODGKIN, A. L. & MCNAUGHTON, P. A. (1980). Temporal and spatial characteristics of the voltage responses of rods in the retina of the snapping turtle. *J. Physiol.* **300**, 213–250.

DUIFHUIS, H. (1976). Cochlear non-linearity and second filter: possible mechanism and implications. *J. acoust. Soc. Am.* **59**, 408–423.

EVANS, E. F. (1972). The frequency response and other properties of single fibres in the guinea-pig cochlear nerve. *J. Physiol.* **226**, 263–287.

EVANS, E. F. & WILSON, J. P. (1973). The frequency selectivity of the cochlea. In *Basic Mechanisms in Hearing*, ed. MOLLER, A. R., pp. 519–554. London & New York: Academic Press.

FEIN, H. (1966). Passing current through recording glass micropipette electrodes. *IEEE Trans. bio-med. Eng.* **13**, 211–212.

FETTIPLACE, R. & CRAWFORD, A. C. (1978). The coding of sound pressure and frequency in cochlear hair cells of the terrapin. *Proc. R. Soc.* B, **203**, 209–218.

FETTIPLACE, R. & CRAWFORD, A. C. (1980). The origin of tuning in turtle cochlear hair cells. *Hearing Res.* **2**, 447–454.

GEISLER, C. D., RHODE, W. S. & KENNEDY, D. T. (1974). Responses to tonal stimuli of single auditory nerve fibres and their relationship to basilar membrane motion in the squirrel monkey. *J. Neurophysiol.* **37**, 1156–1172.

GOLD, T. (1948). Hearing. II. The physical basis of the action of the cochlea. *Proc. R. Soc.* B, **135**, 492–498.

HODGKIN, A. L. & HUXLEY, A. F. (1952). A quantitative description of membrane current and its application to conduction and excitation in nerve. *J. Physiol.* **117**, 500–544.

HOPKINS, C. D. (1976). Stimulus filtering and electroreception: tuberous electroreceptors in three species of Gymnotoid fish. *J. comp. Physiol.* **111**, 171–207.

HUXLEY, A. F. (1959). Ion movements during nerve activity. *Ann. N.Y. Acad. Sci.* **81**, 221–246.

MANLEY, G. A. (1971). Some aspects of the evolution of hearing in vertebrates. *Nature, Lond.* **230**, 506–509.

MANLEY, G. A. (1977). Response patterns and peripheral origin of auditory nerve fibres in the Monitor Lizard, *Varanus bengalensis*. *J. comp. Physiol.* **118**, 249–260.

MAURO, A., CONTI, F., DODGE, F. & SCHOR, R. (1970). Subthreshold behaviour and phenomenological impedance of the squid giant axon. *J. gen. Physiol.* **55**, 497–523.

MILLER, M. R. (1978*a*). Further scanning electron microscope studies of lizard auditory papillae. *J. Morph.* **156**, 381–418.

MILLER, M. R. (1978*b*). Scanning electron microscope studies of the papilla basilaris of some turtles and snakes. *Am. J. Anat.* **151**, 409–436.

MOFFAT, A. J. M. & CAPRANICA, R. R. (1978). Middle ear sensitivity in anurans and reptiles measured by light scattering spectroscopy. *J. comp. Physiol.* **127**, 97–107.

PFEIFFER, R. R. (1970). A model for two-tone inhibition of single cochlear nerve fibres. *J. acoust. Soc. Am.* **48**, 1373–1378.

SZABO, T. (1974). Anatomy of the specialized lateral line organs of electroreception. In *Handbook*

of Sensory Physiology, vol. III/3, *Electroreceptors and Other Specialized Receptors in Lower Vertebrates*, ed. FESSARD, A., pp. 13–58. Heidelberg & New York: Springer Verlag.

WEISS, T. F., MULROY, M. J., TURNER, R. G. & PIKE, C. L. (1976). Tuning of single fibres in the cochlear nerve of the alligator lizard: relation to receptor morphology. *Brain Res.* **115**, 71–90.

WEISS, T. F., PEAKE, W. T., LING, A. & HOLTON, T. (1978). Which structures determine frequency selectivity and tonotopic organisation of vertebrate cochlear nerve fibres? Evidence from the alligator lizard. In *Evoked Electrical Activity in the Auditory Nervous System*. ed. NAUNTON, R. F. & FERNANDEZ, C., pp. 91–112. New York: Academic Press.

WEVER, E. G. (1978). *The Reptile Ear: its Structure and Function*. Princeton University Press.

WILSON, J. P. (1977). Towards a model for cochlear frequency analysis. In *Psychophysics and Physiology of Hearing*, ed. EVANS, E. F. & WILSON, J. P., pp. 115–124. London: Academic Press.